[redacted]

NASA TECHNICAL MEMORANDUM

NASA TM X-74041

COPY NO.

NASA TM X-74041

COMPARISON OF EXPERIMENTAL AND THEORETICAL DRAG CHARACTERISTICS FOR A 10-PERCENT-THICK SUPERCRITICAL AIRFOIL USING A NEW VERSION OF AN ANALYSIS CODE (U)

Charles D. Harris and Dennis O. Allison

Langley Research Center
Hampton, Virginia

NATIONAL SECURITY INFORMATION
Unauthorized Disclosure Subject to
Criminal Sanctions

COMPARISON OF EXPERIMENTAL AND THEORETICAL DRAG CHARACTERISTICS FOR A 10-PERCENT-THICK SUPERCRITICAL AIRFOIL USING A NEW VERSION OF AN ANALYSIS CODE (U)

Charles D. Harris and Dennis O. Allison
Langley Research Center

SUMMARY

A new version of an advanced computer code has recently been developed at the Courant Institute of New York University to analyze two-dimensional transonic flow over an airfoil at high Reynolds numbers. Among the features incorporated into the new version were the addition of a fast solver iteration between every few relaxation iterations which dramatically reduces computation time and a correction to the wave drag formulation which was needed because the computer code uses a nonconservation form of the flow equation.

Drag results obtained with this code are compared with experimental data to assess the ability of the code to predict the drag characteristics of a 10-percent-thick supercritical airfoil at Reynolds numbers from 2 to 11 million. For this airfoil, there remains a tendency for the code to underpredict drag rise Mach number although predicted drag levels are significantly improved by the correction to the wave drag formulation. Also, comments are made concerning various input parameters which may be of interest to users of the computer code.

INTRODUCTION

Reference 1 describes computer codes for the design and analysis of supercritical wing sections. Except for a tendency to overpredict trailing-edge pressure recovery, the analysis code is generally recognized to predict pressure distributions and shock wave locations which agree well with experimental data and has been widely accepted by users in both government and industry.

Drag calculations, however, have tended to overpredict wave losses and have indicated drag rise Mach numbers below that which would be expected from experimental data.

Recent improvements have been made to the analysis code (refs. 2 and 3) which led to a better definition of wave drag and reduced computer time. The purpose of this report is to present a limited comparison of the experimental drag characteristics of a 10-percent-thick supercritical airfoil with characteristics predicted by the improved computer code. The intent is to make available to potential users experimental data suitable for correlation studies and to share with them calculations already performed.

SYMBOLS

Values are given in both the International System of Units (SI) and U.S. Customary Units. Measurements were made in U.S. Customary Units.

c	chord of airfoil, 63.5 cm (25.0 in.)
c_d	section drag coefficient
c_n	section normal-force coefficient
M	Mach number
R_n	Reynolds number based on airfoil chord
x	ordinate along airfoil reference line measured from airfoil leading edge, cm (in.)
z	ordinate normal to airfoil reference line, cm (in.)

COMPUTER CODE PARAMETERS

A complete glossary of computer code parameters is presented in reference 1 except for two new input parameters NFAST and NRELAX. Revised definitions of input parameters which supercede reference 1 will be distributed with the improved code. The following are computer code parameters referred to in this report and are consistent with the revised definitions:

CS	The location of boundary-layer separation computed by the code. Separation is predicted when SEP $\geq$ SEPM.
MxN	The number of mesh intervals in the angular and radial directions in the circle plane at which the flow equations are solved. Default 160 x 30.
NFAST	The number of sweeps through the grid points for each flow cycle using the fast Poisson solver for the subsonic region of the flow. (See NS for definition of flow cycle.) Default 1.
NRELAX	The number of sweeps through the grid points for each flow cycle using the relaxation technique. (See NS for definition of flow cycle.) Default 6.
NS	NS is used along with ITYP on namelist input cards to indicate mode of operation. Also, if NS and ITYP are both positive, NS is the maximum number of flow cycles computed before the next namelist is read. A flow cycle consists of NFAST fast solver iterations plus NRELAX relaxation iterations. Default 1.
NS1	Number of flow cycles computed between boundary-layer calculations. (See NS for definition of flow cycle.) Default 1.

PCH — Chord location at which the turbulent boundary-layer calculation is begun (the laminar boundary layer is neglected). Transition is assumed to occur at this point. Default 0.07.

RDEL — Relaxation parameter for the boundary-layer displacement thickness. Default 0.125.

SEP — Output quantity used as a criterion for determining separation. If SEP > SEPM, the boundary layer separates.

SEPM — Bound imposed on the separation parameter SEP for X < |XSEP|. Also, separation is predicted when SEP > SEPM. Default 0.004.

ST — Convergence tolerance on the maximum velocity potential correction and the maximum circulation correction. ST = 1.E - 5 may be reasonable. ST = 0.0 ensures the completion of NS flow cycles. Default 0.0.

XSEP — For X < |XSEP|, if SEP exceeds SEPM, then the program sets SEP equal to SEPM on the upper surface so that the boundary-layer calculation can proceed through a shock wave. For X > |XSEP|, SEP is free to exceed SEPM to allow separation to be properly predicted. If XSEP is negative, the upper and lower surfaces are both treated as upper surfaces. Default 0.93.

THEORETICAL DRAG

Old Version of Analysis Code

An airfoil analysis code developed by Garabedian, et al (ref. 1), based on a nonconservation form (NCF) of the equation for the velocity potential

describing transonic flow, has gained wide acceptance for the prediction of two-dimensional pressure distributions. This code has been distributed by the Langley Research Center through the Computer Software Management and Information Center (COSMIC) and will be referred to hereafter as the "old" analysis code.

As discussed by Garabedian (refs. 2 and 3),however, the NCF method fell short of giving an adequate prediction of drag rise Mach numbers because of erroneous positive terms in the artificial viscosity. The shock jumps defined by the NCF method created mass instead of conserving it (see also, ref. 4) resulting in overprediction of the wave drag, especially in the case of large supersonic zones.

New Version of Analysis Code

A correction has recently been made to this "old" analysis code to account for the mass generated by the NCF method (refs. 2 and 3) which leads to a more satisfactory evaluation of the wave drag. In addition to the corrected wave drag formulation, an accelerated iteration scheme developed by Jameson (ref. 5) has been incorporated to reduce computation time (ref. 3).

In the old analysis code, the equations for transonic flow were solved iteratively through a relaxation technique. A series of relaxation iterations were performed with the boundary layer being updated every few iterations. Each relaxation iteration was considered to be an iterative "cycle". Jameson found that the rate of convergence could be increased by adding a fast solver over the subsonic flow region between every NRELAX relaxation iterations. An iterative "cycle" then becomes a combination of NFAST fast solvers and NRELAX relaxation iterations with the boundary layer being updated between every NSYS "cycles".

This new version of the code, incorporating the corrected wave drag formulation and reduced computing time, is referred to hereafter as the "new" analysis code. It is also distributed through COSMIC as program number LAR-12265.

Drag Calculations

From the viewpoint of a user with only limited knowledge of the mathematical basis of the code, two questions naturally arise: how well does the new analysis code predict drag, and to what extent can the code be used in a cookbook fashion by letting certain input parameters assume their default values?

In order to provide insight into these questions, drag characteristics have been calculated with the new analysis code for comparison with experimental data for a 10-percent-thick NASA supercritical airfoil. In addition, the effects of a limited number of input parameters were investigated. Although detailed analysis of these effects were not made, the results are useful in demonstrating the sensitivity of the code to certain parameters and provide systematic data for further correlation studies.

EXPERIMENTAL DRAG

The experimental drag characteristics of a 10-percent-thick NASA supercritical airfoil are presented in figure 1 for various normal-force coefficients at Reynolds numbers from 2 to 11 x 10^6. An expanded drag scale is used in this and subsequent figures to make it easier to differentiate between curves. Such an expanded scale, however, tends to exaggerate differences and this must be kept in mind.

The experimental data were determined from wake-survey measurements utilizing a rake of total head tubes during experiments in the Langley 8-foot transonic pressure tunnel with the two-dimensional airfoil model spanning the tunnel. The airfoil was a heretofore unpublished supercritical airfoil developed for a normal-force coefficient of about 0.5 and identified as supercritical airfoil 27. Transition was fixed at 5 percent on both the upper and lower surfaces. Measured model coordinates are presented in table I.

RESULTS AND DISCUSSION

The analysis code has 33 namelist parameters which include physical inputs such as the boundary-layer transition point (PCH) and abstract inputs such as the maximum number of flow cyles (NS), the convergence tolerance (ST), the boundary-layer relaxation parameter (RDEL), and the number of mesh intervals (MxN). These input parameters may be specified by the user or allowed to assume values specified by the computer code (default values).

Calculated results presented in this report are based on various combinations of the following values of NS, RDEL, and MxN: NS from 20/10 (crude/fine grid) to 50/25; RDEL = 0.125 and 0.070; and MxN = 160 x 30 and 108 x 20. ST = 5×10^{-6} for all calculations. Other abstract input parameters were allowed to assume their default values.

Physical inputs such as Mach number, Reynolds number, and boundary-layer transition point are set equal to their experimental values. Section lift coefficient is set equal to the experimental section normal-force coefficient since the angle of attack was small (from -1° to 1°) for all cases considered.

Basic Drag Comparison

Figures 2 to 4 show comparisons between the experimental drag characteristics and the drag as calculated by the new analysis code for normal-force coefficients of 0.40, 0.50, and 0.60. The calculations were performed at Mach numbers corresponding to those for which experimental data were available with NS = 40/20 (RDEL and MXN assumed their default values). Total drag values (profile + wave) as calculated without the wave-drag correction term are shown (+ symbols) on the figures to indicate the magnitude of the wave-drag correction incorporated into the new analysis code.

The number of iterative cycles (40 crude/20 fine) was chosen somewhat arbitrarily in the absence of a definitive study of their effects. The effects of varying the number of iterative cycles were later studied and the results are discussed in a subsequent section of this report. According to that study, NS = 40/20 were more than enough cycles.

The convergence tolerance (ST) of 5×10^{-6} which was used for all calculations was, in general, never achieved except for M = 0.60 where there were no supersonic zones. The code, therefore, except for M = 0.60, generally ran the full 40/20 iterative cycles. The values of the velocity potential correction (DPHI) and the circulation correction (DCL) at the end of 40/20 cycles typically were on the order of 5×10^{-4} to 5×10^{-5}.

One abstract input parameter, XSEP, was monitored during the calculations of the theoretical data of figures 2 to 4 to assure that its upper surface chordwise location (LP) was ahead of the predicted location of separation (CS). Thus, for a few conditions where separation occurred slightly ahead of the default value of XSEP = 0.93, the code was rerun with XSEP = 0.90 and the results indicated by flagged symbols in figures 2 to 4.

As may be seen from figures 2 to 4, the theory often predicts a few counts of negative wave drag (where the dashed line is below the solid line) at the lower Mach numbers. Since negative wave drag is physically unreal, it will be excluded (assumed equal to zero) in all remaining calculated results (figs. 5 to 9). The advantage of excluding negative wave drag is best seen in figure 4 for the normal-force coefficient of 0.60.

The experimental-theoretical drag comparisons shown in figure 3 for the near design normal-force coefficient of 0.50 are repeated in figure 5 with the negative wave drag excluded. Estimated values of the experimental profile drag are also shown. In general, drag correlation at the lower Mach numbers where the flow is entirely subsonic or where zones of supersonic flow are just beginning to develop is good. Discrepancies at the highest Reynolds number for low Mach numbers are due to the fact that laminar flow could not be maintained experimentally through the leading-edge pressure peaks which occur ahead of the transition strip.

At M = 0.60 and $R_n = 11 \times 10^6$, for example, transition probably takes place at the leading-edge pressure coefficient peak which occurs near the 2-percent chord resulting in the experimental drag being about 4 counts (0.0004) higher than the analysis code predicts with PCH = 0.05. Moving the location at which the turbulent boundary-layer begins on the upper surface forward to PCH (upper) = 0.02 (requiring only a minor modification to the analysis code)

would add 4 counts of profile drag to the theoretical drag and bring the theoretical drag into agreement with experimental drag (not presented). It is important, therefore, that the location of boundary-layer transition be correctly specified on both the upper and lower surfaces in order for the analysis code to accurately predict drag.

At higher Mach numbers where zones of supersonic flow have developed, agreement is not as good as at the lower Mach numbers, particularly at the lowest Reynolds number of 2×10^6 (fig. 5(a)). Figure 5 suggests that the code's semiempirical treatment of the turbulent boundary layer does not adequately model the thick boundary layers at the lower Reynolds numbers and results in a slight overprediction of both profile and wave drag. In general, agreement improves with increasing Reynolds numbers.

The theoretical drag at $M = 0.82$ and $R_n = 11 \times 10^6$ (fig. 5(d)) does not fit the general pattern, however, since it is well below the experimental drag. The discrepancy is believed to be associated with the relaxation parameter RDEL default value of 0.125 which allows each succeeding boundary layer to exert too much of an influence and results in fluctuations in the boundary layer and calculated drag. This becomes important for flows where the shock wave has moved near the trailing edge and increased in strength. At $M = 0.82$, for example, the shock is at the 75-percent chord station and has a strong influence on the boundary layer at the trailing edge. Such fluctuations are illustrated in figure 6 where drag values for different values of NS (fine) are presented. It is believed, therefore, that a smaller value of RDEL would be appropriate.

Reduced RDEL and Mesh Size

Figure 7 shows the effects of reducing the relaxation parameter for the boundary-layer displacement thickness (RDEL) from its default value of 0.125 to 0.070 and the effects of reducing the number of mesh intervals by approximately one-third in each direction. The smaller value of RDEL tended to dampen boundary-layer displacement thickness fluctuations between cycles (not presented), smooth the drag characteristics (fig. 7), and hasten convergence. Pressure distributions were not significantly affected by reducing RDEL.

Reducing the number of mesh intervals from MxN = 160 x 30 to 108 x 20 tended to have the same general effects as reducing RDEL; boundary-layer displacement thickness fluctuations were dampened and drag characteristics were smoothed. The coarser mesh resulted in reductions in computing time of approximately 50 percent for flows with supersonic zones. The pressure distributions calculated with MxN = 108 x 20 were essentially the same as for MxN = 160 x 30 except that shock wave locations tended to be 1 to 2 percent of the chord further rearward, and the shock waves were slightly more smeared with the coarser mesh.

Thus, where computer capacity is limited or where computing time is a factor, the coarser mesh could be utilized without a significant loss in accuracy as long as drag rather than shock wave definition was of primary importance.

Number of Iterative Cycles

Figure 8 shows the effects of number of iterative cycles at selected conditions for RDEL values of 0.125 and 0.070. There is some variation in the drag with the number of iterative cycles and with RDEL at the lowest Reynolds number ($R_n = 2 \times 10^6$) where the boundary layer is thicker and its influence more pronounced. At the higher Reynolds numbers, it appears to make little difference how many cycles are used. To further verify this, a comparison was made over the Reynolds number and Mach number range of the experimental data for NS = 40/20 and 20/10 iterative cycles with RDEL = 0.125 at $c_n = 0.50$ and is presented in figure 9.

Because of the smoother drag characteristics with RDEL = 0.070 (fig. 7), it seemed more desirable to use RDEL = 0.070 rather than 0.125. Intuitively, however, 20/10 cycles might not be enough cycles to achieve good resolution of the boundary layer with RDEL = 0.070, particularly at low Reynolds numbers. For airfoils thicker than 10 percent where gradients would be steeper and boundary-layers thicker, further intuitive justification for more than 20/10 cycles might be argued. Therefore, drag data were generated with an intermediate number of cycles, 30/15, for RDEL = 0.070 and included in figure 9.

Overall, the NS = 30/15, RDEL = 0.070 data more nearly approximates the experimental data. However, if plotted to a more conventional scale, the three theoretical curves of figure 9 would be practically indistinguishable.

Drag Divergence Mach Numbers

Although significant improvements in drag calculations were made (figs. 2 to 4), there remains a tendency for the new analysis code to slightly overpredict drag in the vicinity of the drag divergence Mach number at the near design normal-force coefficient of 0.50 (fig. 9). Thus, the theoretical drag rise occurs somewhat earlier than the experimental data would indicate. This discrepancy varies with Reynolds number from roughly $\Delta M = 0.02$ at the lowest Reynolds number to $\Delta M = 0.01$ at the highest Reynolds number.

Agreement between experimental and theoretical drag rise characteristics seemed to be better at lower normal-force coefficients. At the lower, off-design normal-force coefficient of 0.40, for example, correlation was very good at the higher test Reynolds numbers (figs. 2(c) and 2(d)).

CONCLUDING REMARKS

A comparison between experimental drag characteristics and theoretical drag characteristics derived from an improved analysis code for a 10-percent-thick supercritical airfoil at Reynolds numbers from 2 to 11 million indicate the following general conclusions:

1. There was significant improvement in predicted drag characteristics compared with the "old" analysis code due to reformulation of wave drag.

2. There remains a tendency for the new code to overpredict drag in the vicinity of drag divergence Mach numbers resulting in early drag rise predictions at the near-design normal-force coefficient of 0.5. This discrepancy in drag rise Mach number varies with Reynolds number from about 0.02 at $R_n = 2 \times 10^6$ to 0.01 at $R_n = 11 \times 10^6$.

3. At the lower, off-design normal-force coefficient of 0.4 good drag rise Mach number correlation was evidenced at the higher test Reynolds numbers.

4. It appears that a good cookbook method of applying the new code is to run 30 crude cycles and 15 fine cycles, set the boundary-layer relaxation parameter equal to 0.07, let the number of mesh intervals assume the default value of 160 x 30, and exclude any negative wave drag from the total drag.

5. Where precise shock wave definition is not of primary importance, appreciable savings in computer time may be realized with little effect on the drag characteristics by a one-third reduction in the default number of mesh intervals in each direction.

REFERENCES

1. Bauer, F.; Garabedian, P.; Korn, D.; and Jameson, A.: Supercritical Wing Sections II. Lecture Notes in Economics and Mathematical Systems, M. Beckmann and H. P. Kunzi, eds., Springer-Verlag, 1975.

2. Garabedian, P. R.: Computation of Wave Drag for Transonic Flow. J. d'Analyse Mathematique, vol. 30, 1976, pp. 164-171.

3. Garabedian, P. R.: Transonic Flow Theory of Airfoils and Wings. Advances in Engineering Science , vol. 4, NASA CP-2001, 1976.

4. Newman, Perry A.; and South, Jerry C., Jr.: Conservative Versus Nonconservative Differencing: Transonic Streamline Shape Effects. NASA TM X-72827, 1976.

5. Jameson, A.: Accelerated Iteration Schemes for Transonic Flow Calculations Using Fast Poisson Solvers. ERDA Research and Development Rep. COO-3077-82, Courant Inst. of Mathematical Sciences, New York Univ., March 1975.

Table I

Coordinates for 10-Percent-Thick Supercritical Airfoil 27

x/c	$(z/c)_{upper}$	$(z/c)_{lower}$
0	0	0
.005	.0122	-.0112
.010	.0163	-.0151
.020	.0212	-.0202
.03	.0244	-.0236
.04	.0269	-.0263
.05	.0290	-.0286
.06	.0308	-.0306
.07	.0324	-.0324
.08	.0339	-.0340
.09	.0352	-.0355
.10	.0364	-.0368
.11	.0375	-.0380
.12	.0385	-.0391
.13	.0395	-.0401
.14	.0404	-.0410
.15	.0412	-.0419
.16	.0420	-.0427
.17	.0427	-.0434
.18	.0434	-.0441
.19	.0440	-.0447
.20	.0446	-.0453
.21	.0452	-.0459
.22	.0457	-.0464
.23	.0462	-.0469
.24	.0466	-.0474
.25	.0470	-.0478
.26	.0474	-.0482
.27	.0477	-.0485
.28	.0480	-.0488
.29	.0483	-.0491
.30	.0486	-.0493
.31	.0488	-.0495
.32	.0490	-.0497
.33	.0492	-.0498
.34	.0494	-.0499
.35	.0496	-.0500
.36	.0497	-.0500
.37	.0498	-.0500
.38	.0499	-.0500
.39	.0500	-.0499
.40	.0500	-.0498

x/c	$(x/c)_{upper}$	$(z/c)_{lower}$
.41	.0500	-.0497
.42	.0500	-.0495
.43	.0500	-.0493
.44	.0500	-.0491
.45	.0499	-.0488
.46	.0498	-.0485
.47	.0497	-.0481
.48	.0496	-.0477
.49	.0495	-.0473
.50	.0493	-.0468
.51	.0491	-.0463
.52	.0489	-.0457
.53	.0487	-.0450
.54	.0485	-.0442
.55	.0482	-.0434
.56	.0479	-.0425
.57	.0476	-.0415
.58	.0473	-.0404
.59	.0470	-.0392
.60	.0466	-.0380
.61	.0462	-.0367
.62	.0458	-.0353
.63	.0454	-.0338
.64	.0450	-.0322
.65	.0445	-.0305
.66	.0440	-.0287
.67	.0435	-.0269
.68	.0430	-.0250
.69	.0424	-.0231
.70	.0418	-.0212
.71	.0412	-.0193
.72	.0406	-.0174
.73	.0399	-.0155
.74	.0392	-.0136
.75	.0385	-.0117
.76	.0377	-.0098
.77	.0369	-.0080
.78	.0361	-.0062
.79	.0352	-.0045
.80	.0343	-.0028
.81	.0333	-.0013
.82	.0323	.0001
.83	.0312	.0014

Table I. - Continued.

x/c	$(z/c)_{upper}$	$(z/c)_{lower}$
.84	.0301	.0026
.85	.0289	.0036
.86	.0277	.0045
.87	.0264	.0052
.88	.0250	.0057
.89	.0235	.0060
.90	.0219	.0061
.91	.0202	.0061
.92	.0184	.0059
.93	.0165	.0054
.94	.0145	.0046
.95	.0124	.0035
.96	.0102	.0021
.97	.0079	.0004
.98	.0055	-.0016
.99	.0029	-.0039
1.00	-.0002	-.0066

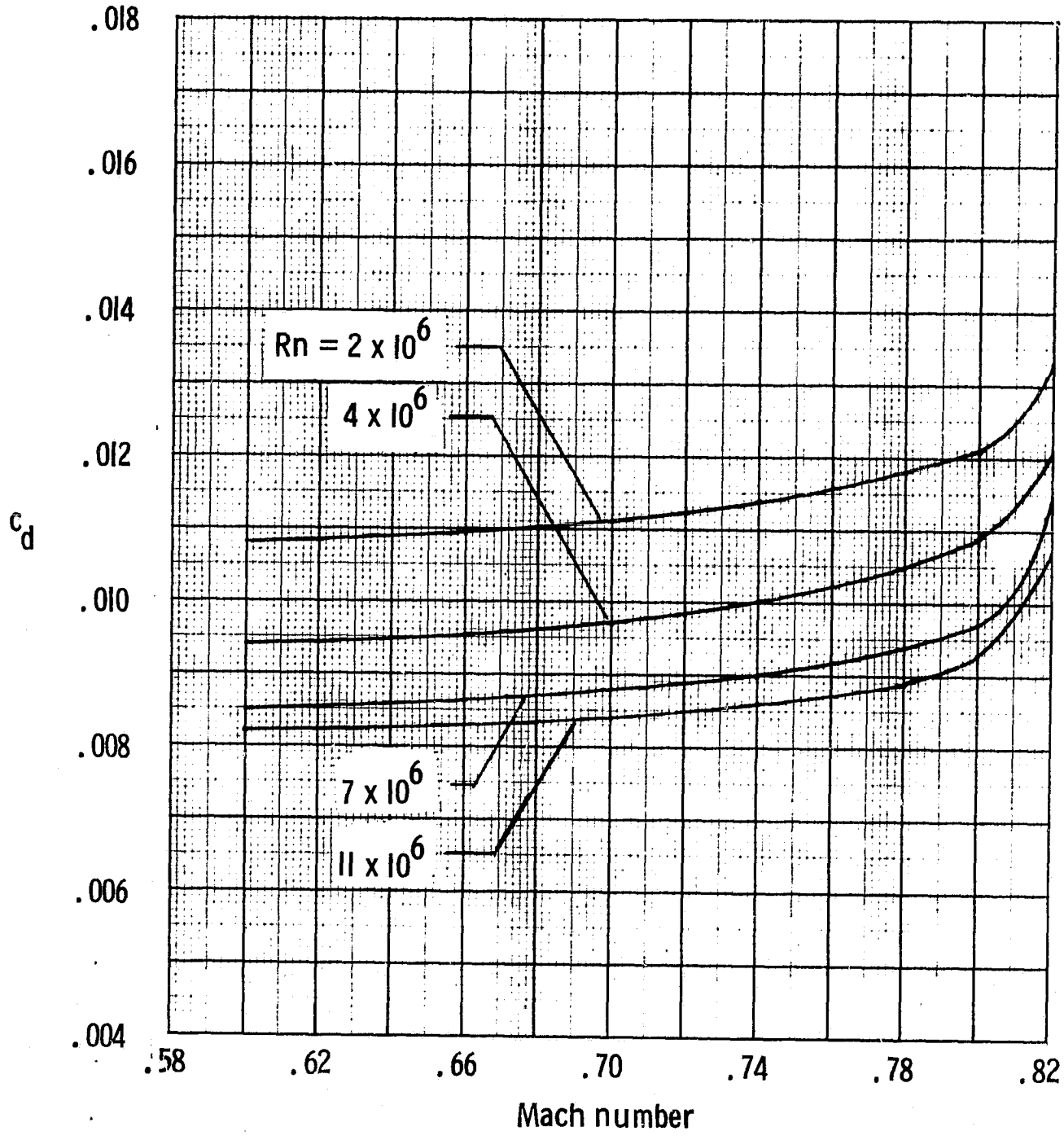

(a) $c_n = 0.40$

Figure 1. - Variation of experimental section drag coefficient with Mach number for 10-percent-thick supercritical airfoil 27.

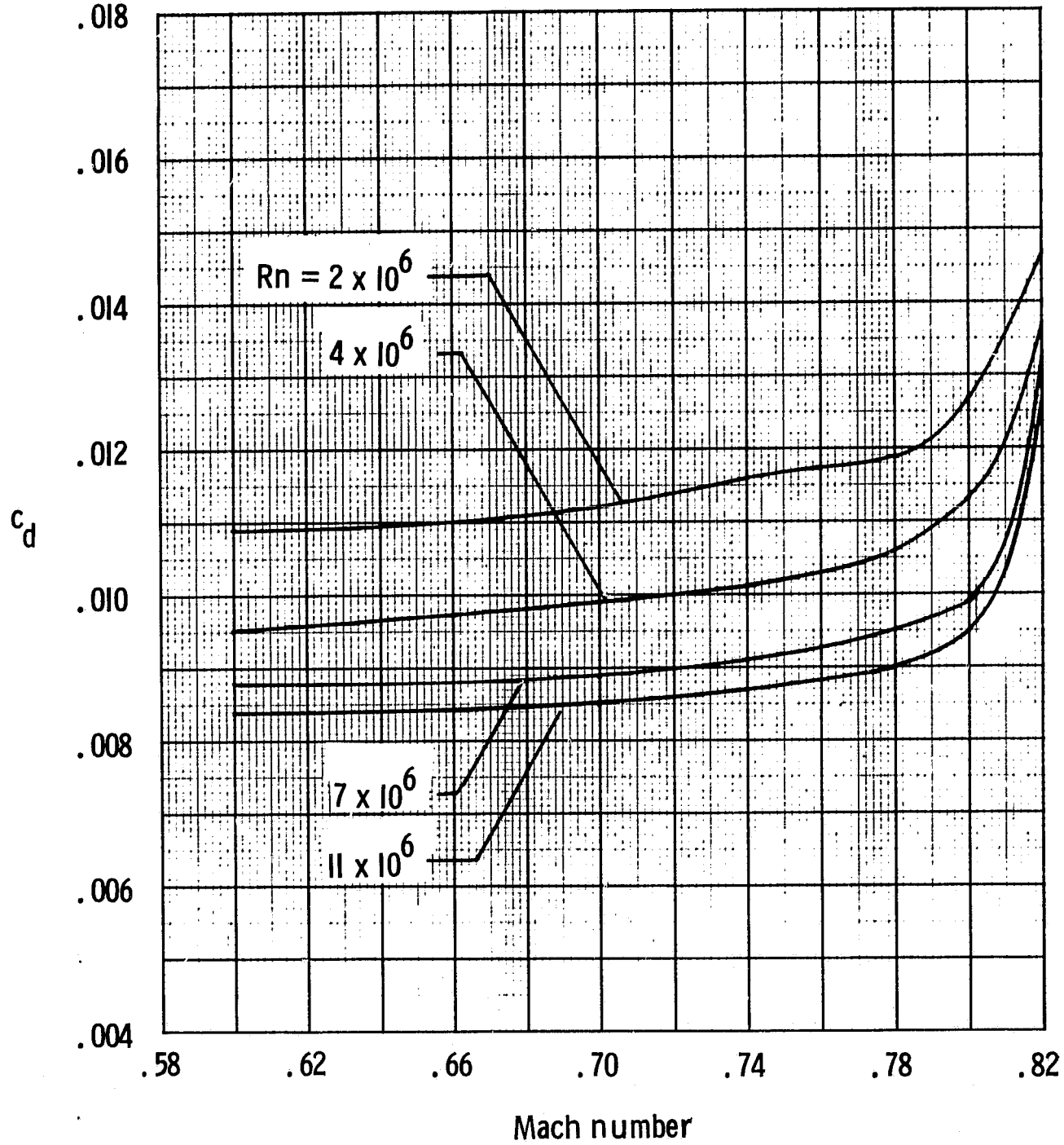

(b) $c_n = 0.50$

Figure 1. - Continued.

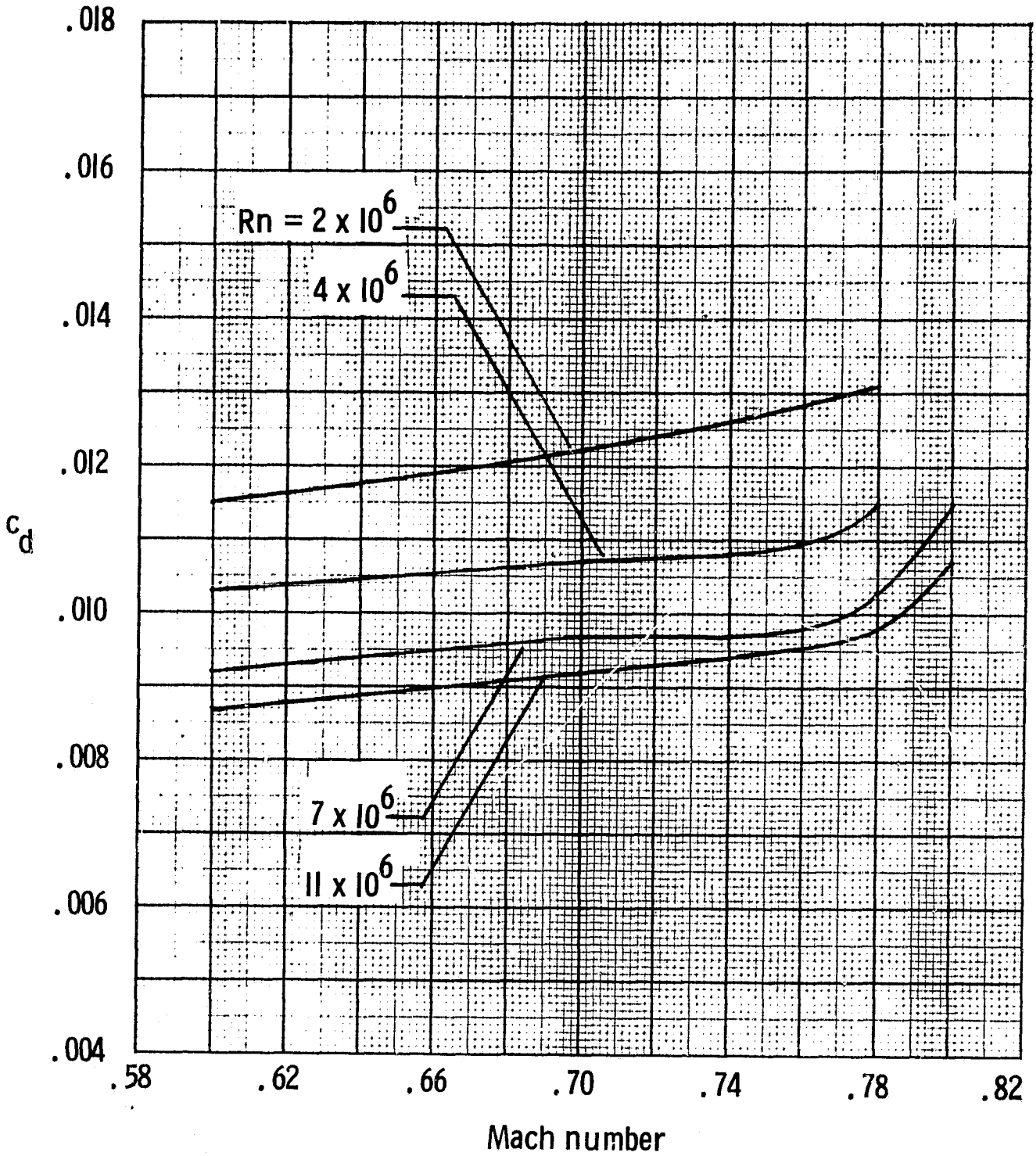

(c) c_n = 0.60

Figure 1. - Continued.

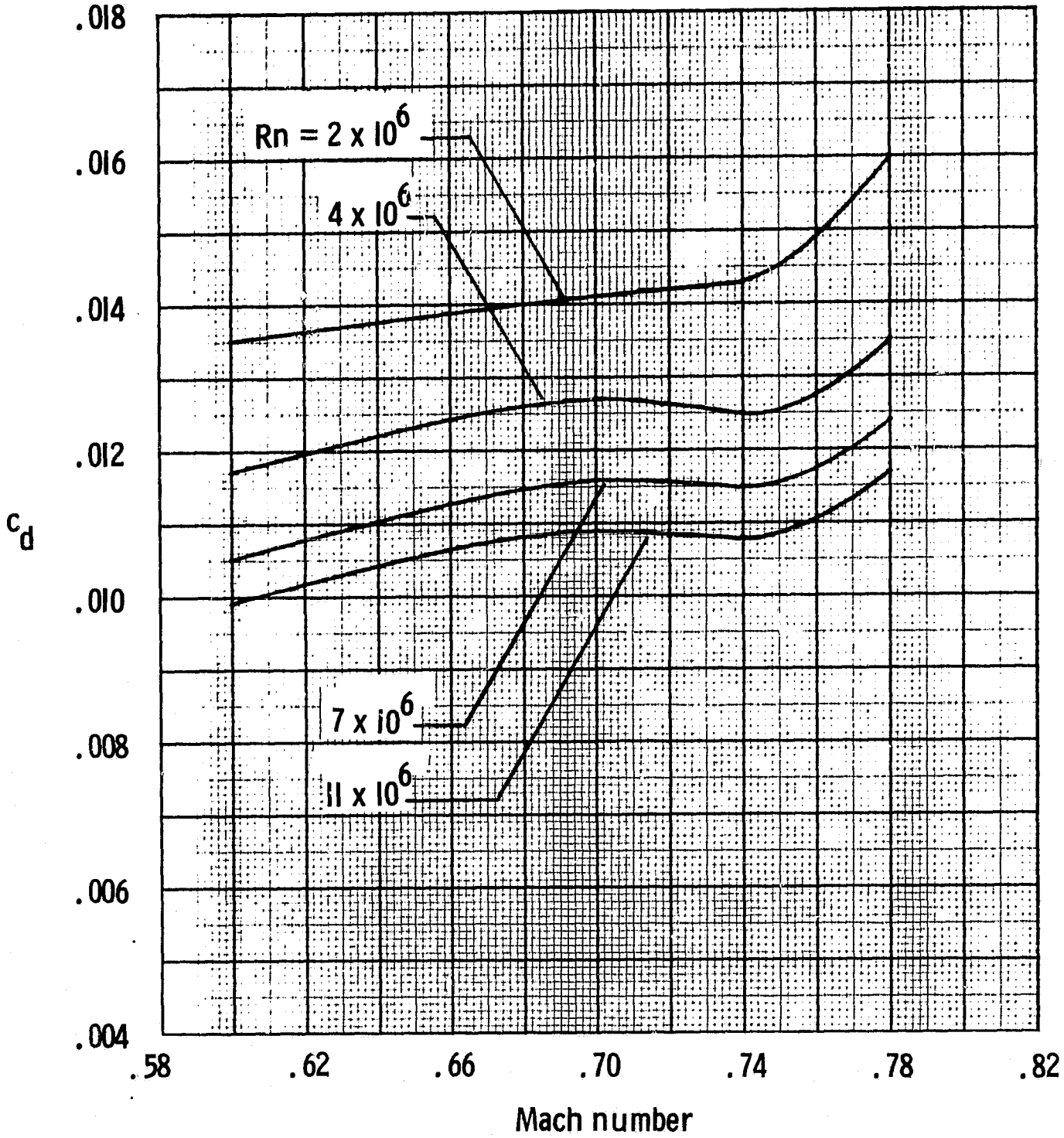

(d) $c_n = 0.70$

Figure 1. - Concluded.

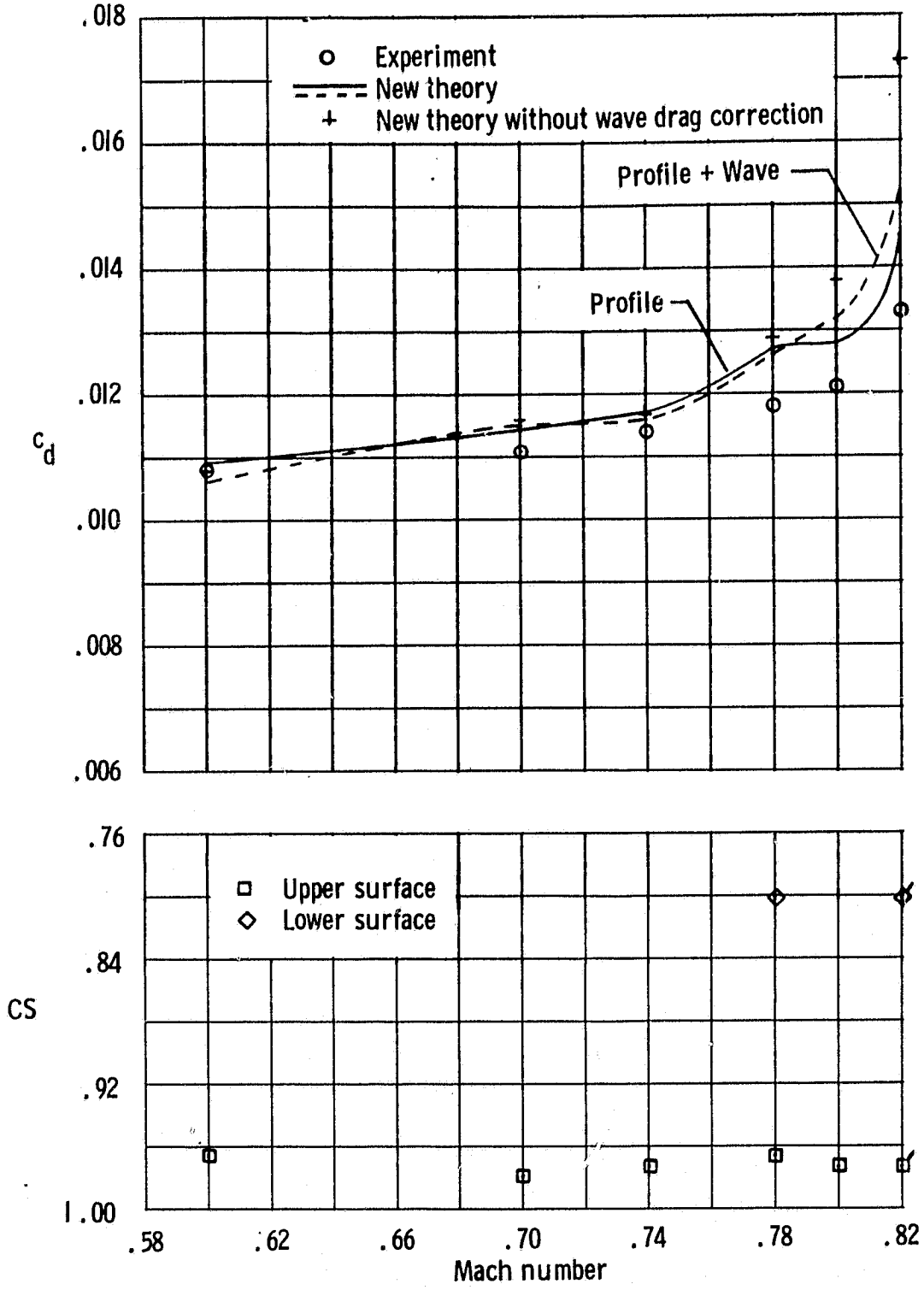

(a) $R_n = 2 \times 10^6$

Figure 2. - Comparison of experimental and theoretical drag characteristics and theoretical separation characteristics. c_n = 0.40; PCH = 0.05; MxN = 160 x 30, NS(crude) = 40; NS(fine) = 20; RDEL = 0.125; XSEP = 0.93. Flagged symbols indicate Mach numbers for which XSEP = 0.90.

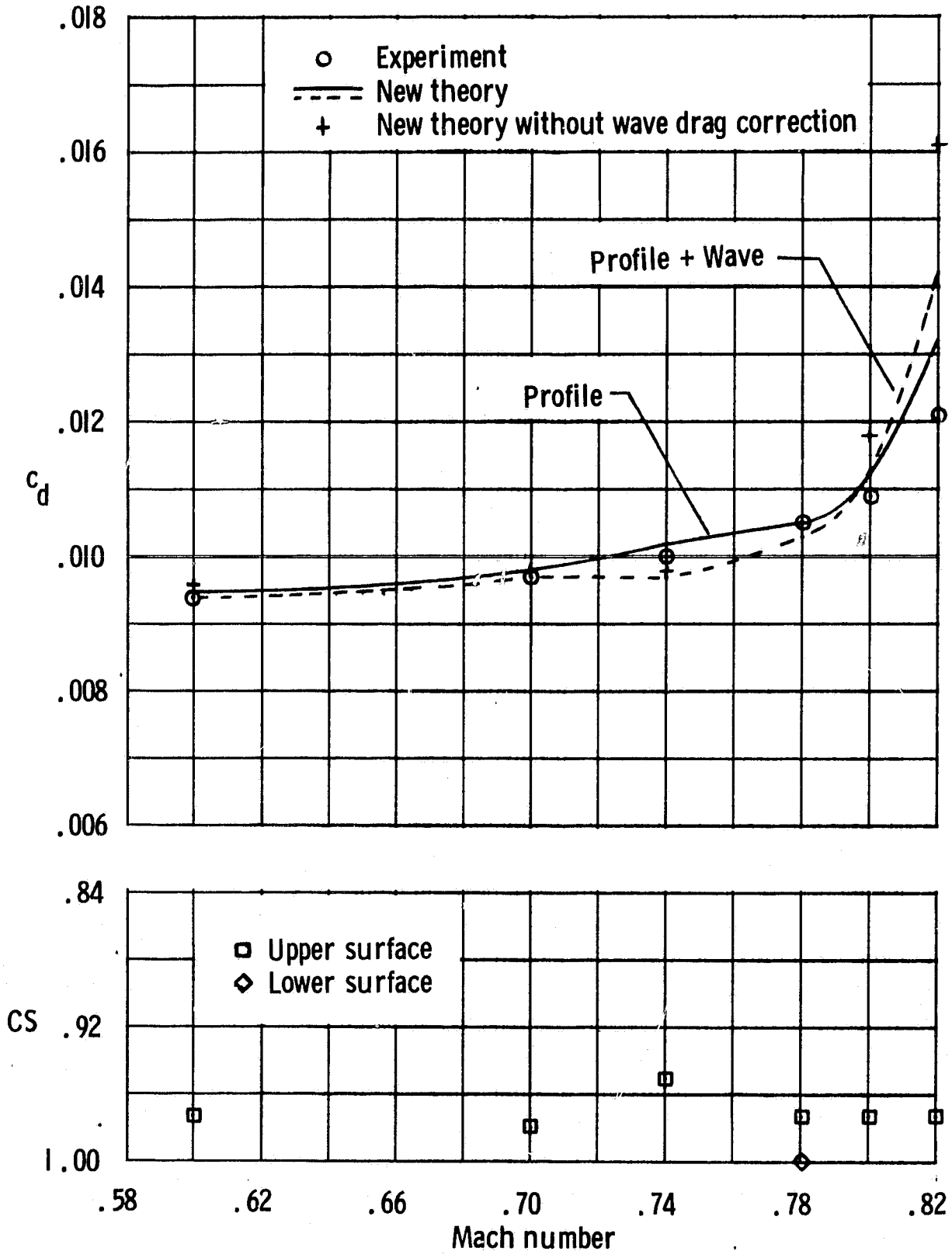

(b) $R_n = 4 \times 10^6$

Figure 2. - Continued.

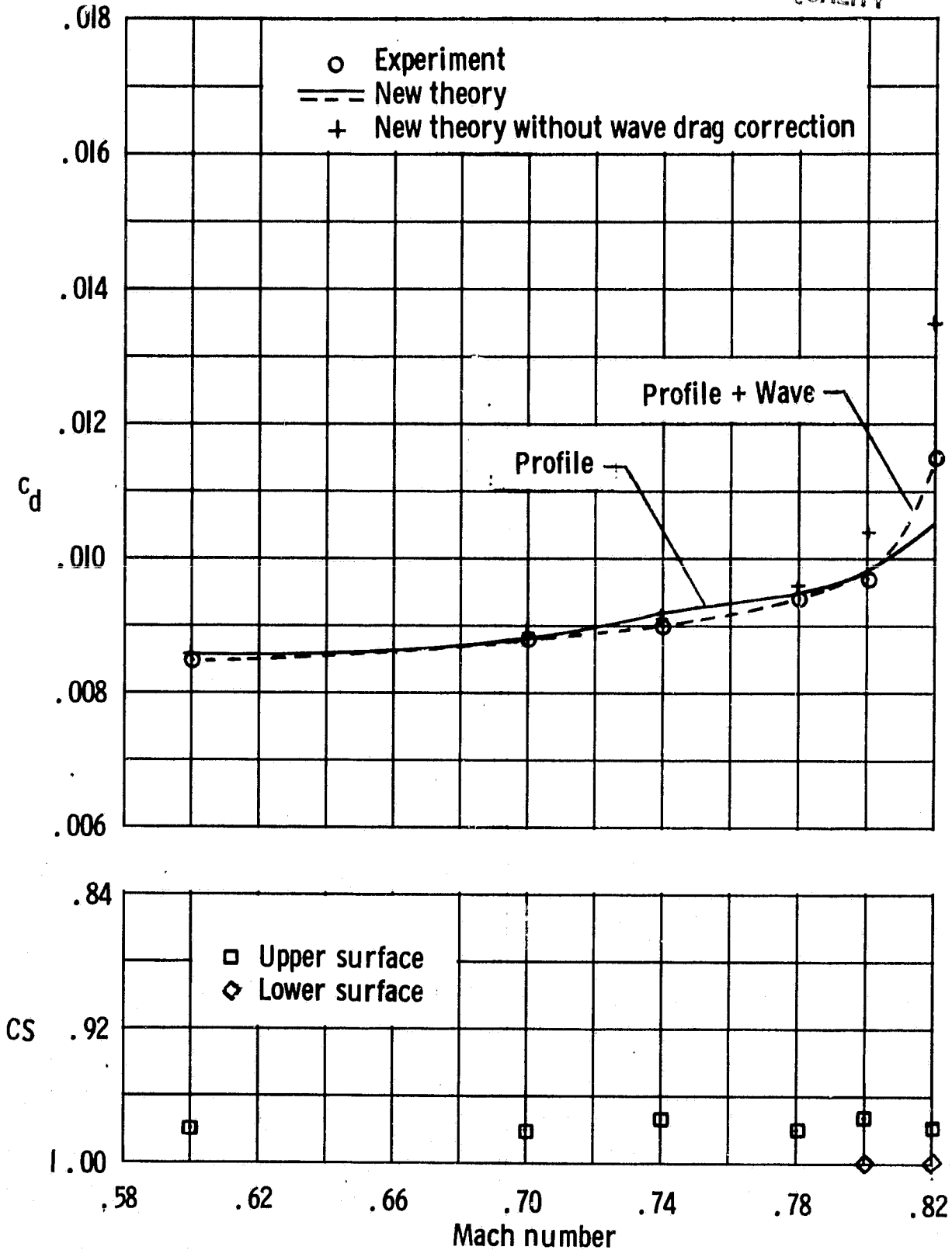

(c) $R_n = 7 \times 10^6$

Figure 2. - Continued.

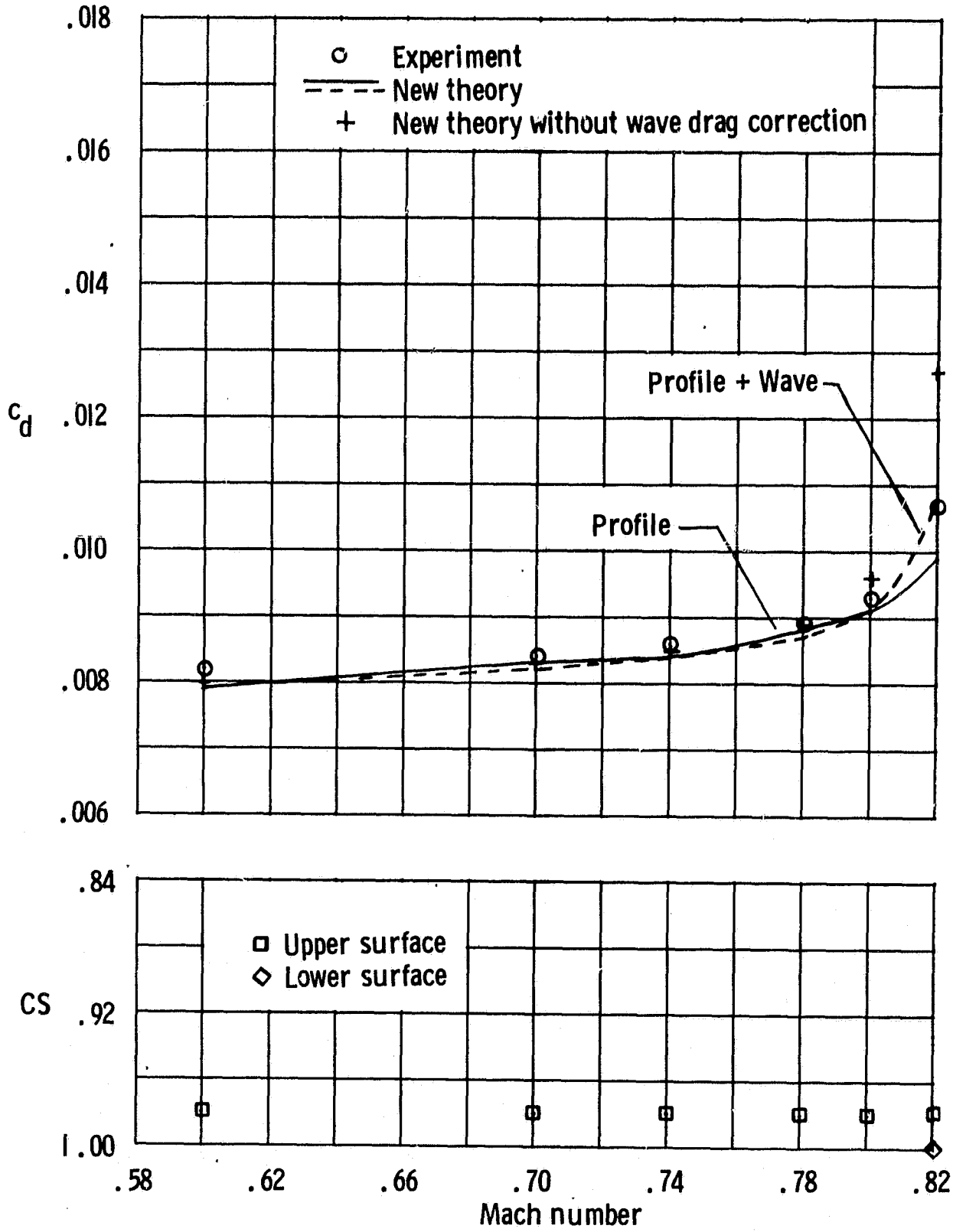

(d) $R_n = 11 \times 10^6$

Figure 2. - Concluded.

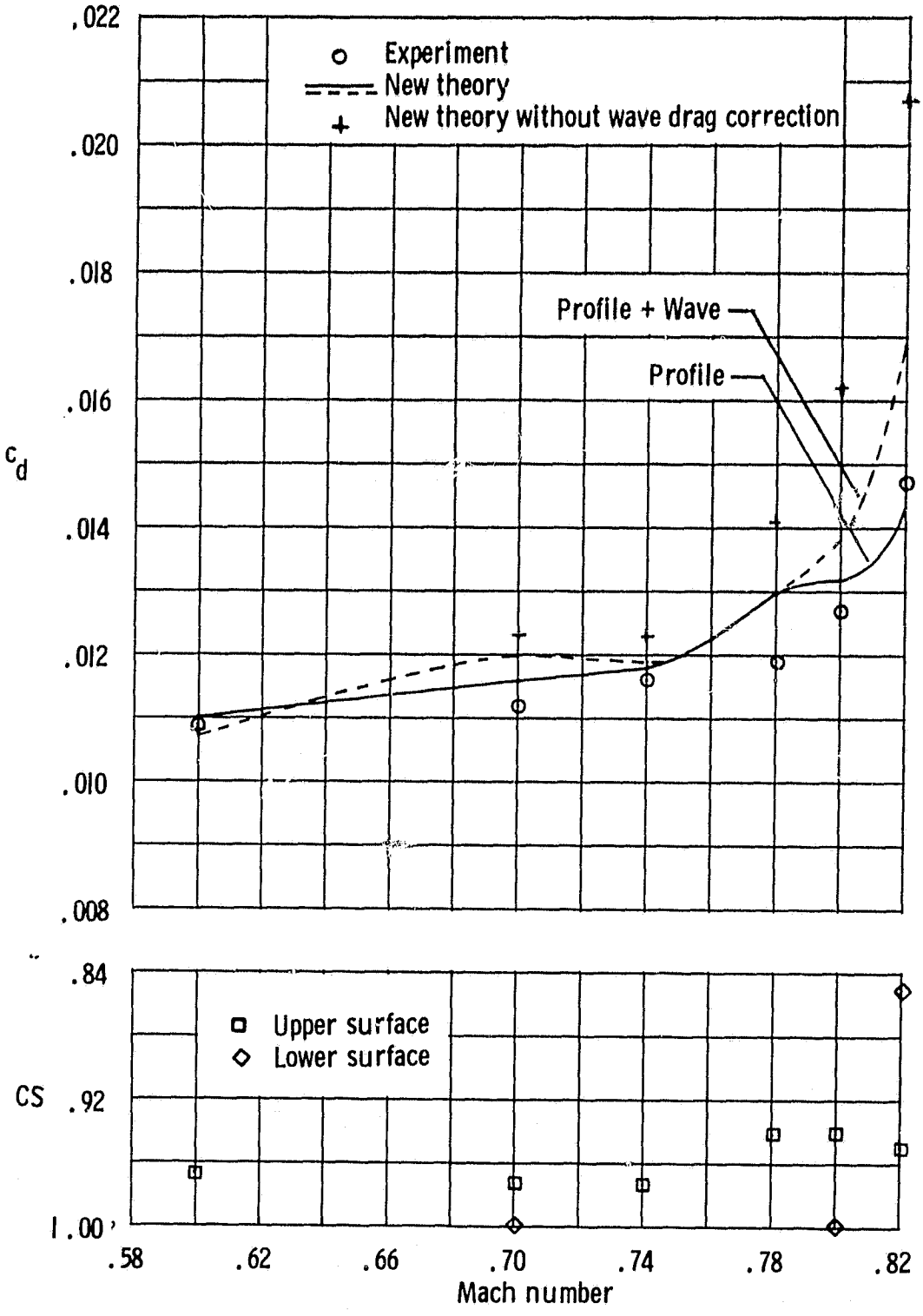

(a) $R_n = 2 \times 10^6$

Figure 3. - Comparison of experimental and theoretical drag characteristics and theoretical separation characteristics. c_n = 0.50; PCH = 0.05; MxN = 160 x 30; NS(crude) = 40; NS(fine) = 20; RDEL = 0.125; XSEP = 0.93. Flagged symbols indicate Mach numbers for which XSEP = 0.90.

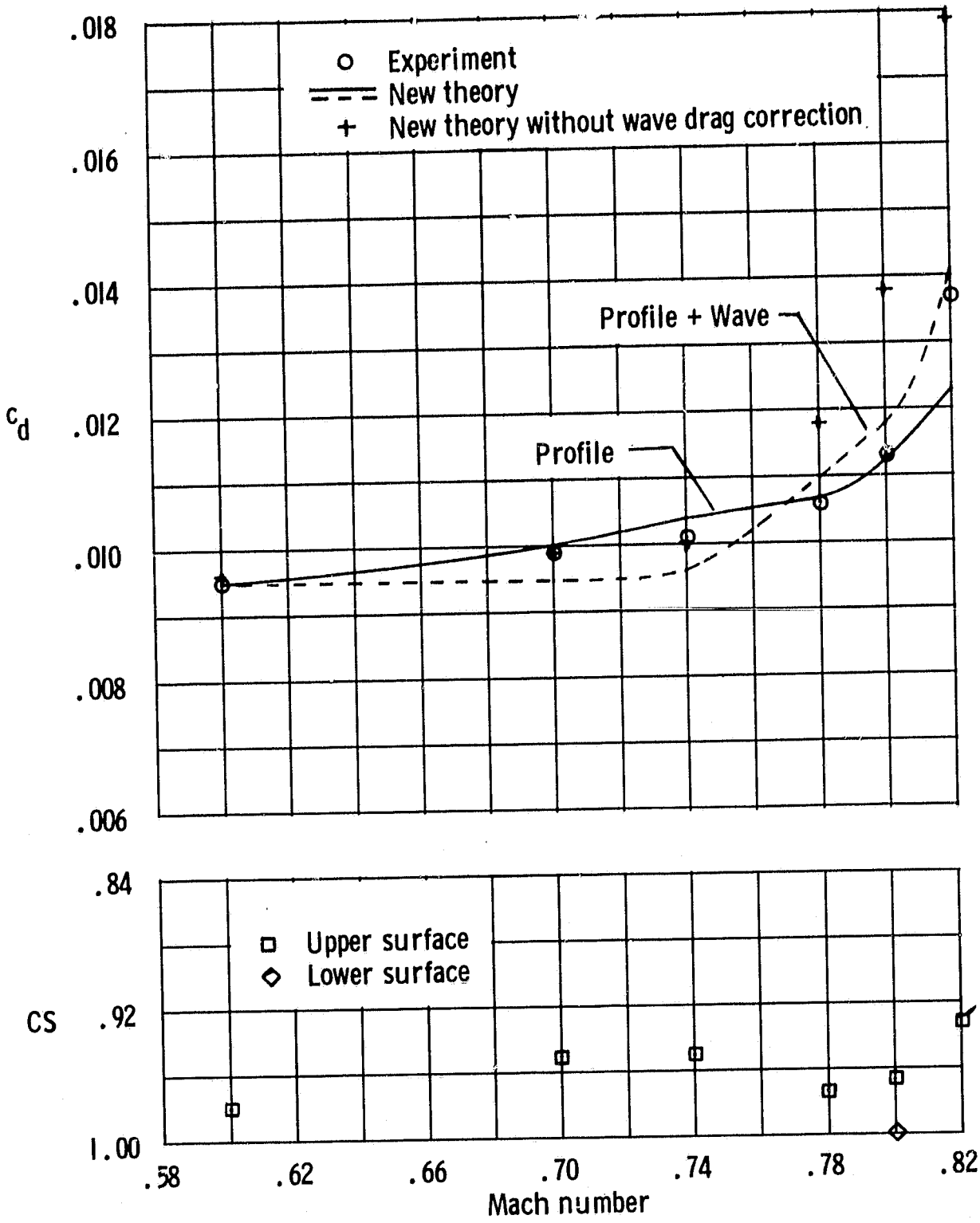

(b) $R_n = 4 \times 10^6$

Figure 3. - Continued.

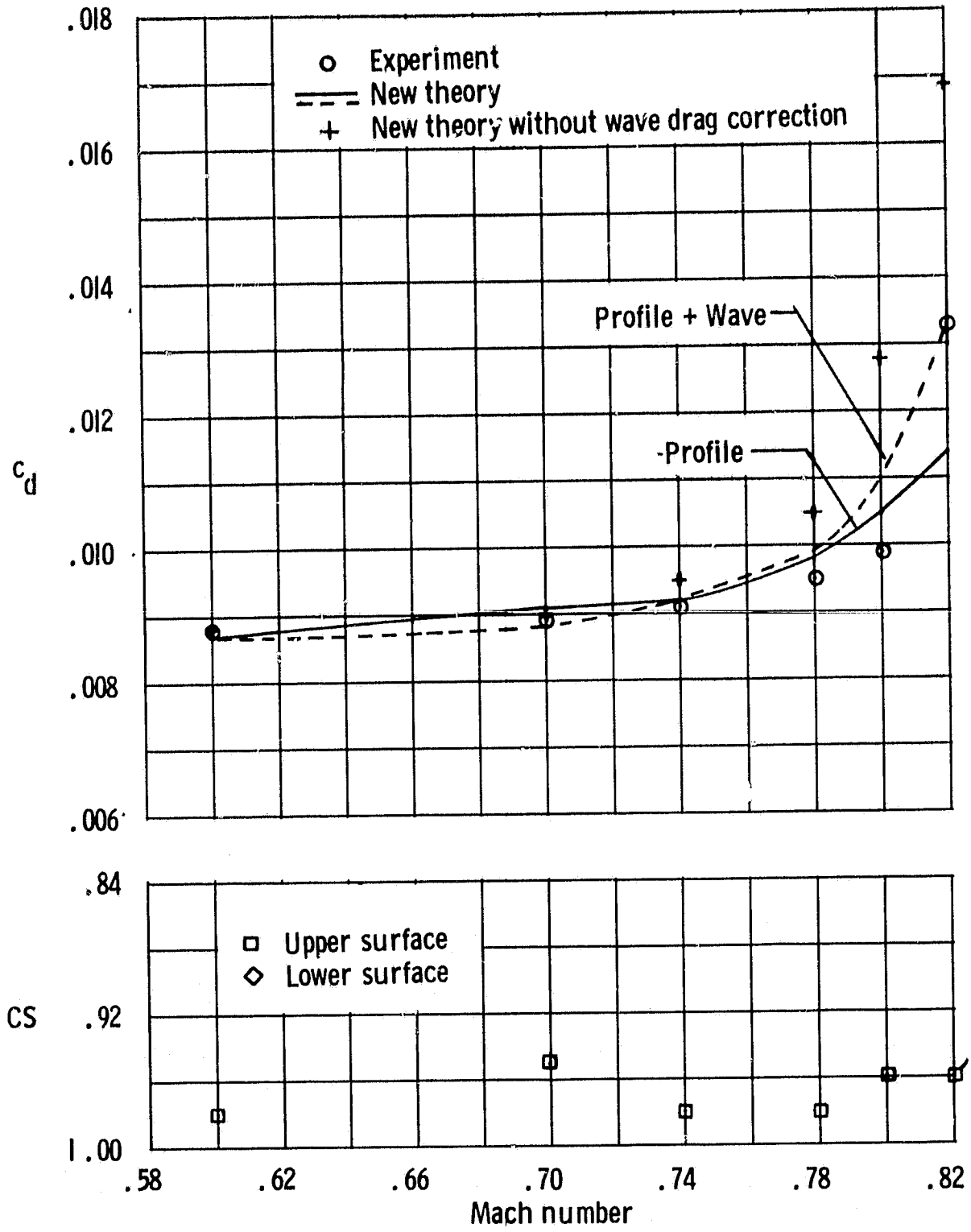

(c) $R_n = 7 \times 10^6$

Figure 3. - Continued.

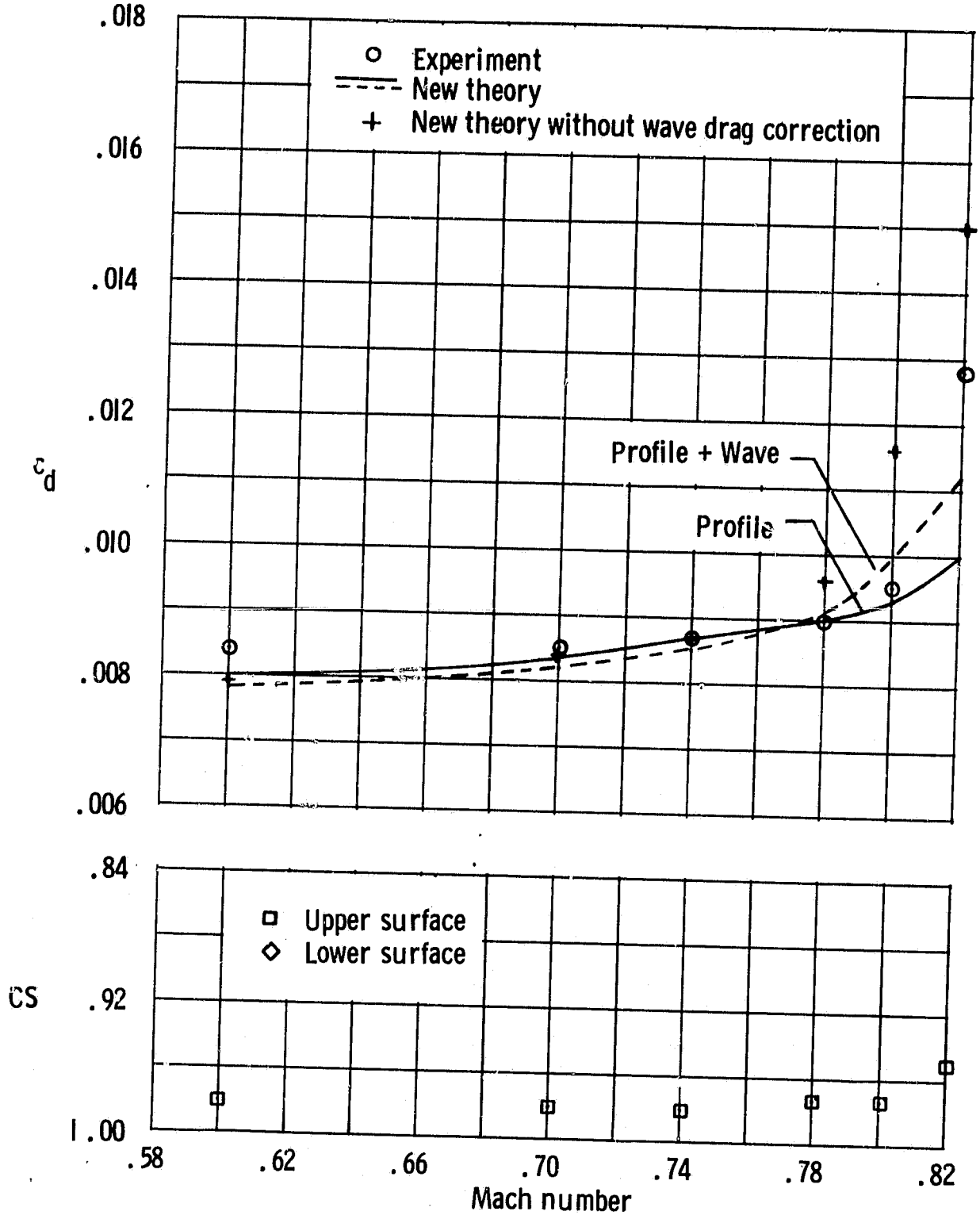

(d) $R_n = 11 \times 10^6$

Figure 3. - Concluded.

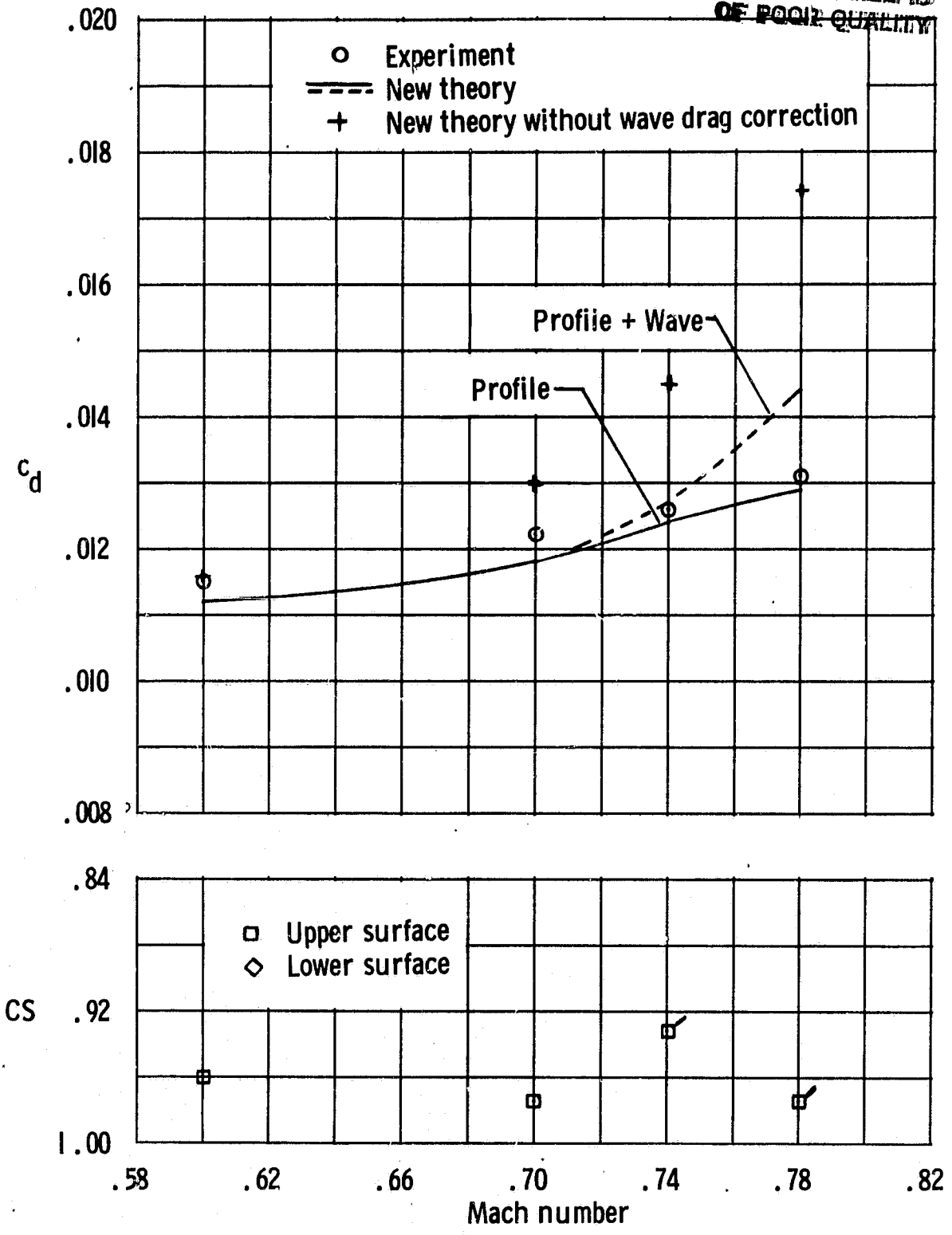

(a) $R_n = 2 \times 10^6$

Figure 4. - Comparison of experimental and theoretical drag characteristics and theoretical separation characteristics. c_n = 0.60; PCH = 0.05; MxN = 160 x 30; NS(crude) = 40; NS(fine) = 20; RDEL = 0.125; XSEP = 0.93. Flagged symbols indicate Mach numbers for which XSEP = 0.90.

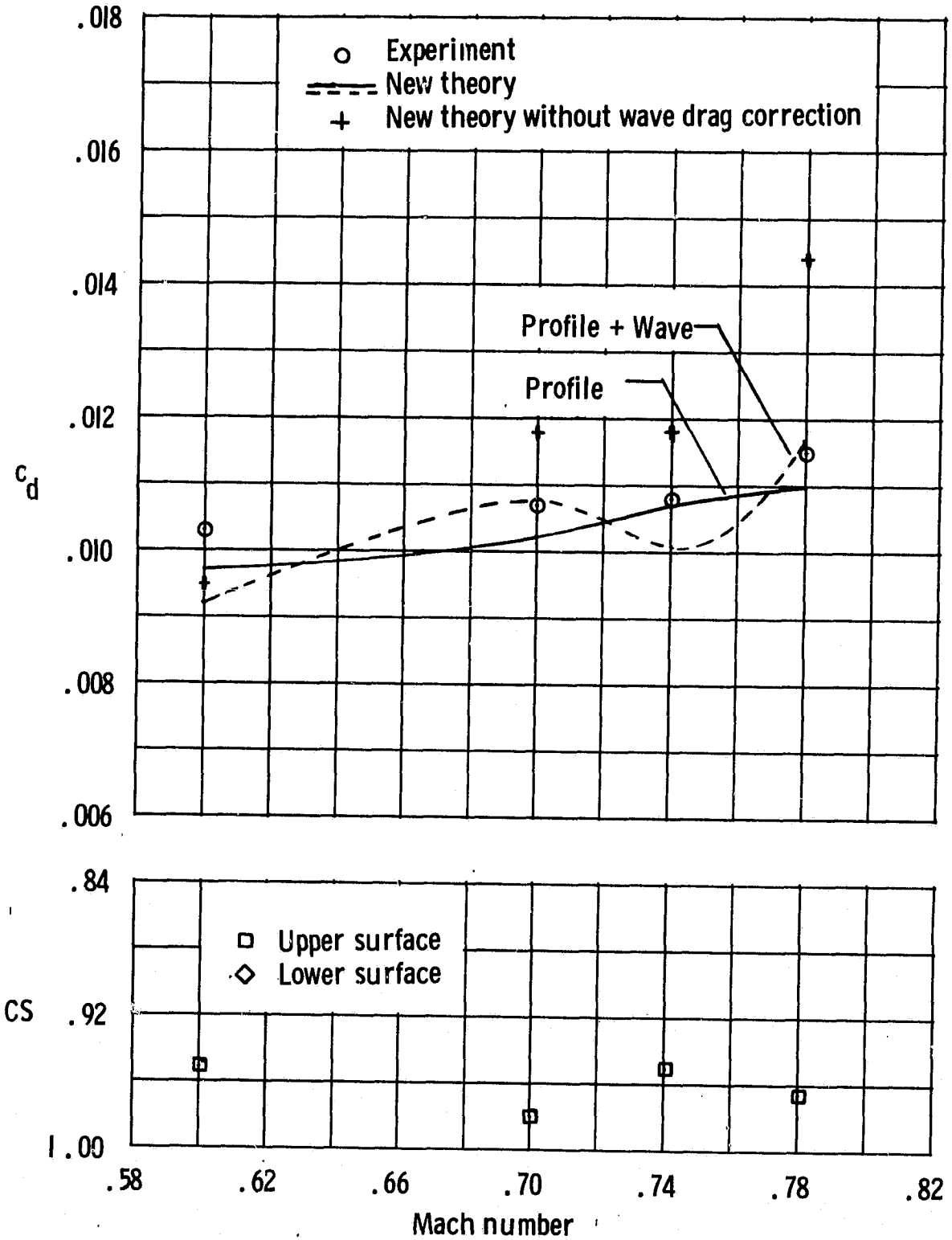

(b) $R_n = 4 \times 10^6$

Figure 4. - Continued.

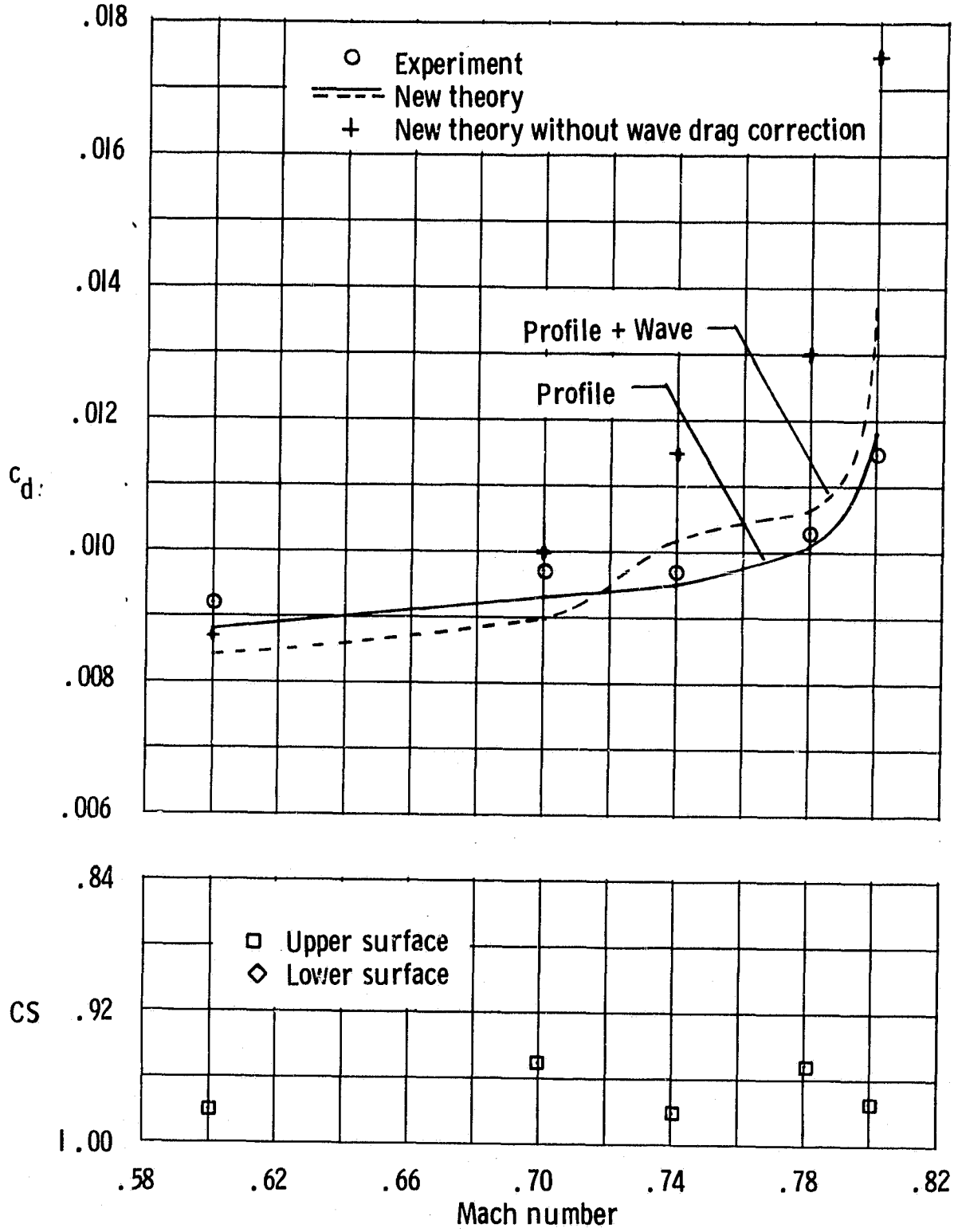

(c) $R_n = 7 \times 10^6$

Figure 4. - Continued.

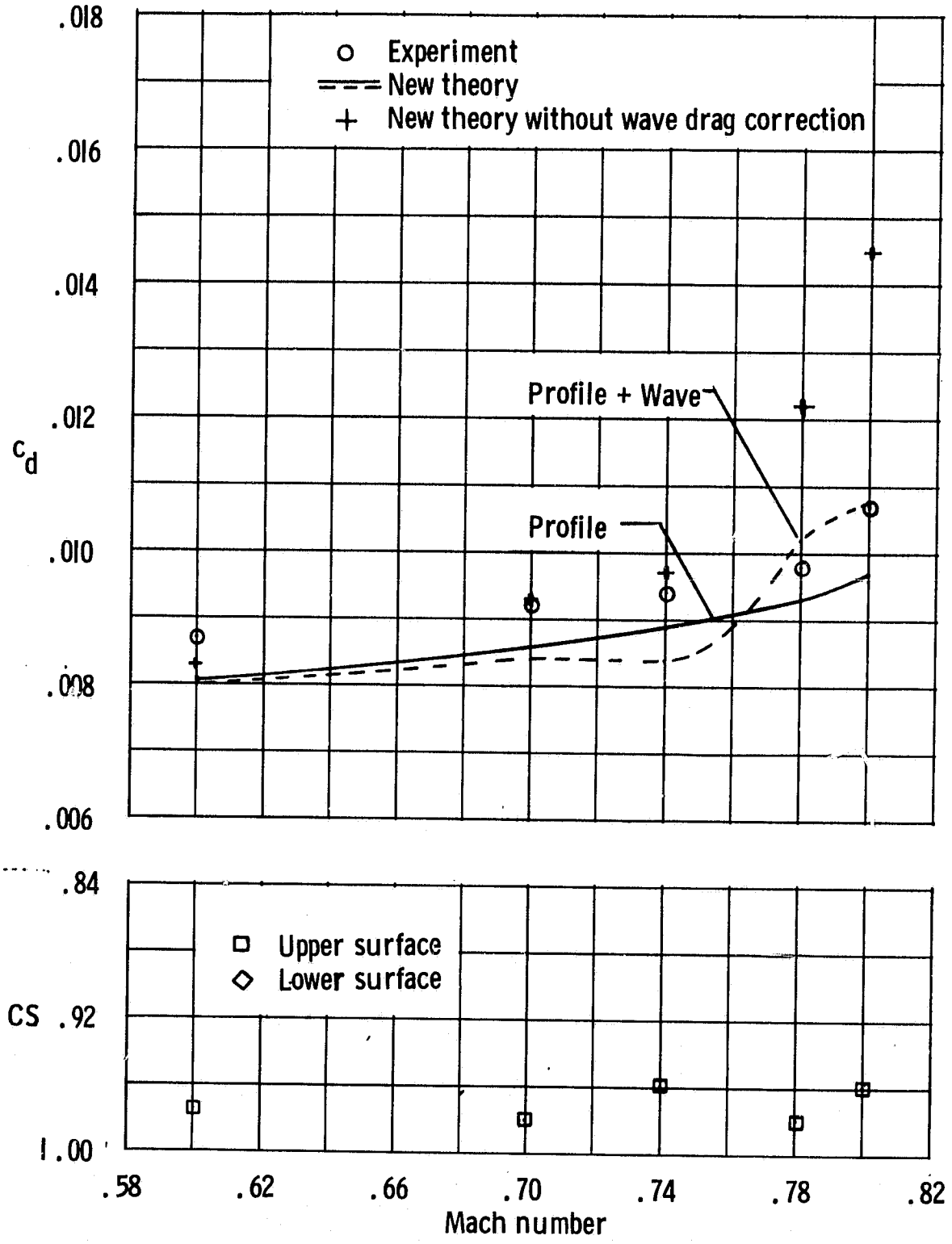

(d) $R_n = 11 \times 10^6$

Figure 4. - Concluded.

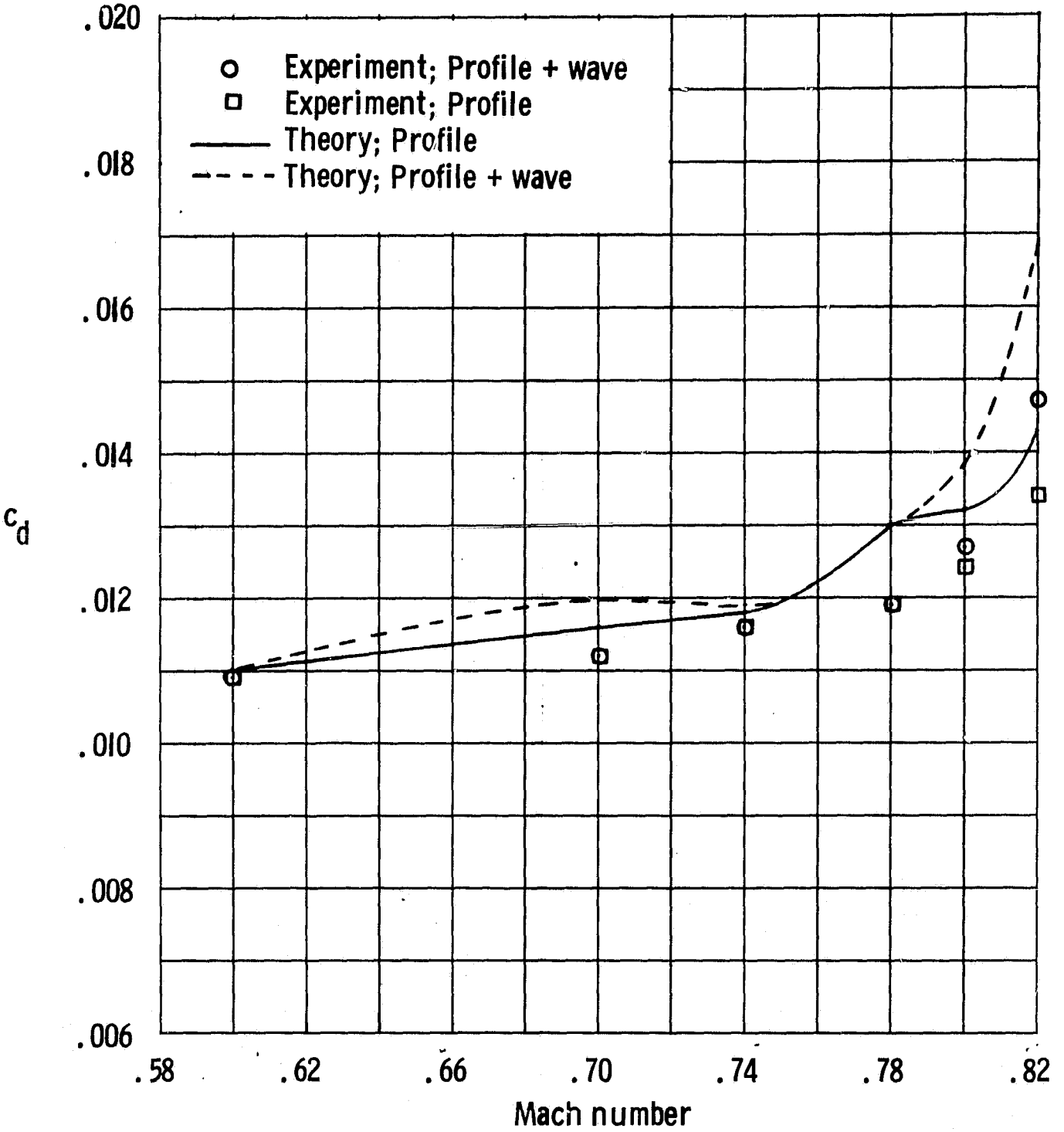

(a) $R_n = 2 \times 10^6$

Figure 5. - Comparison of experimental and theoretical drag characteristics. $c_n = 0.50$; PCH = 0.05; MxN = 160 x 30; NS(crude) = 40; NS(fine) = 20; RDEL = 0.125; negative wave drag excluded.

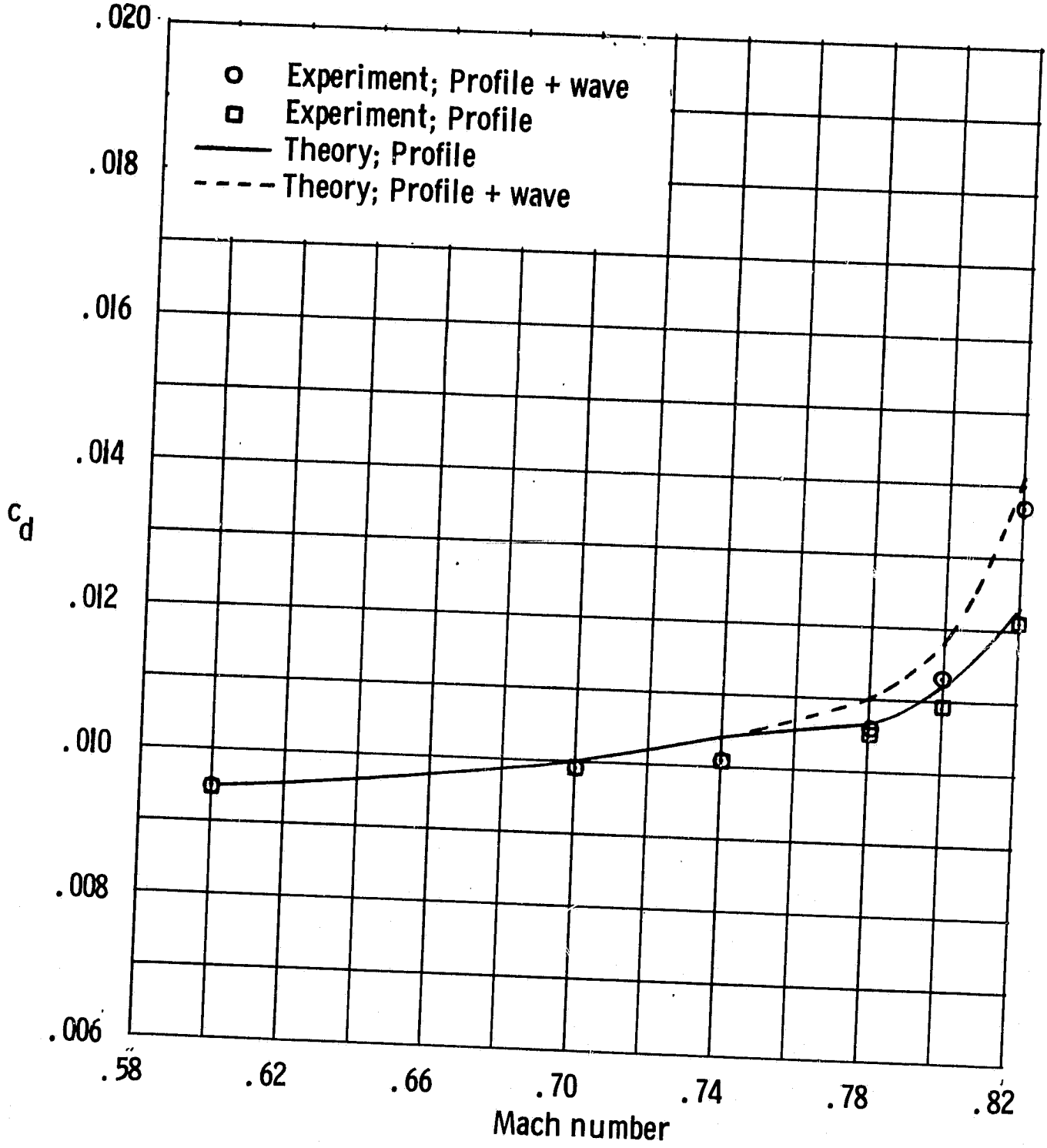

(b) $R_n = 4 \times 10^6$

Figure 5. - Continued.

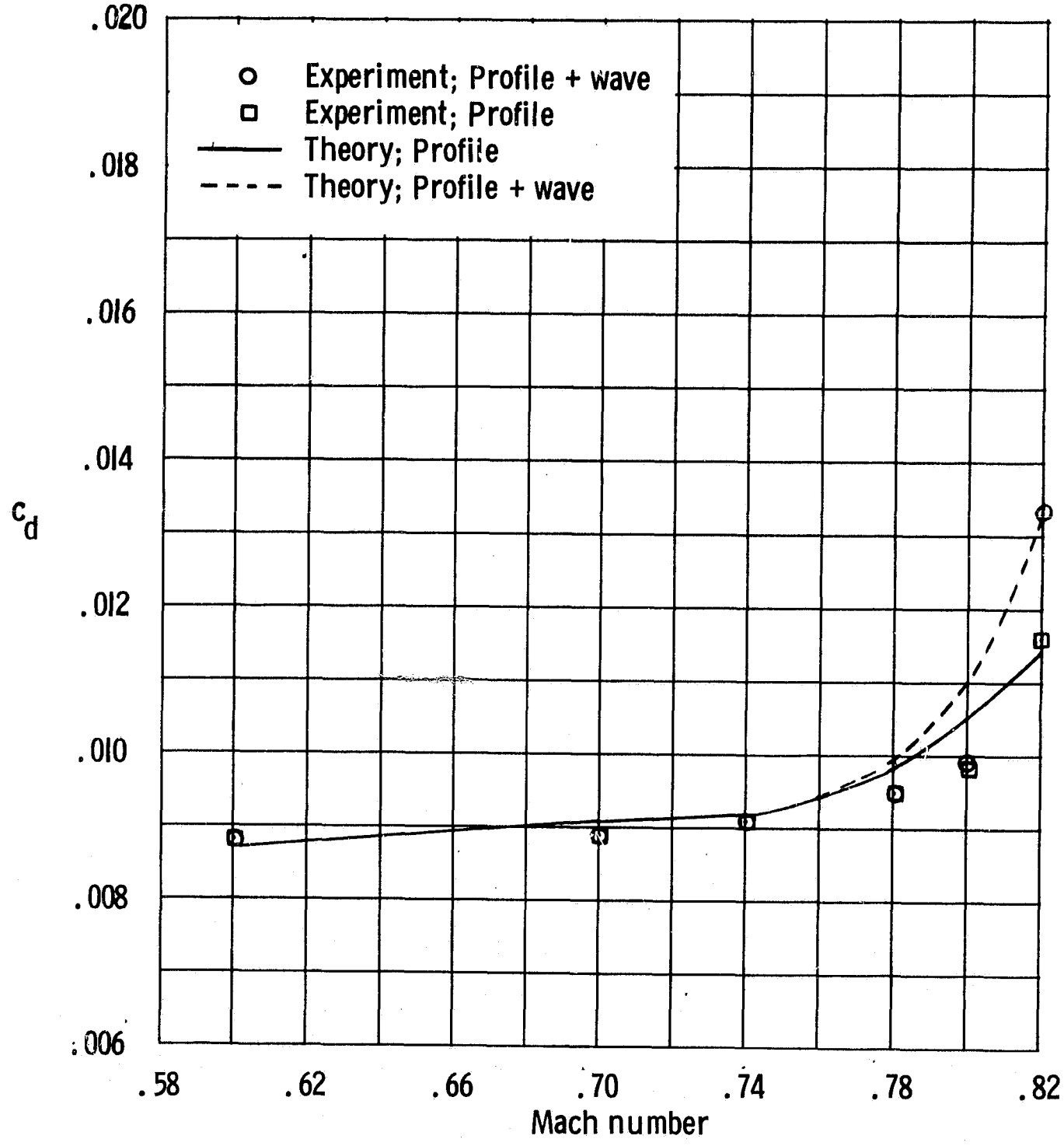

(c) $R_n = 7 \times 10^6$

Figure 5. - Continued.

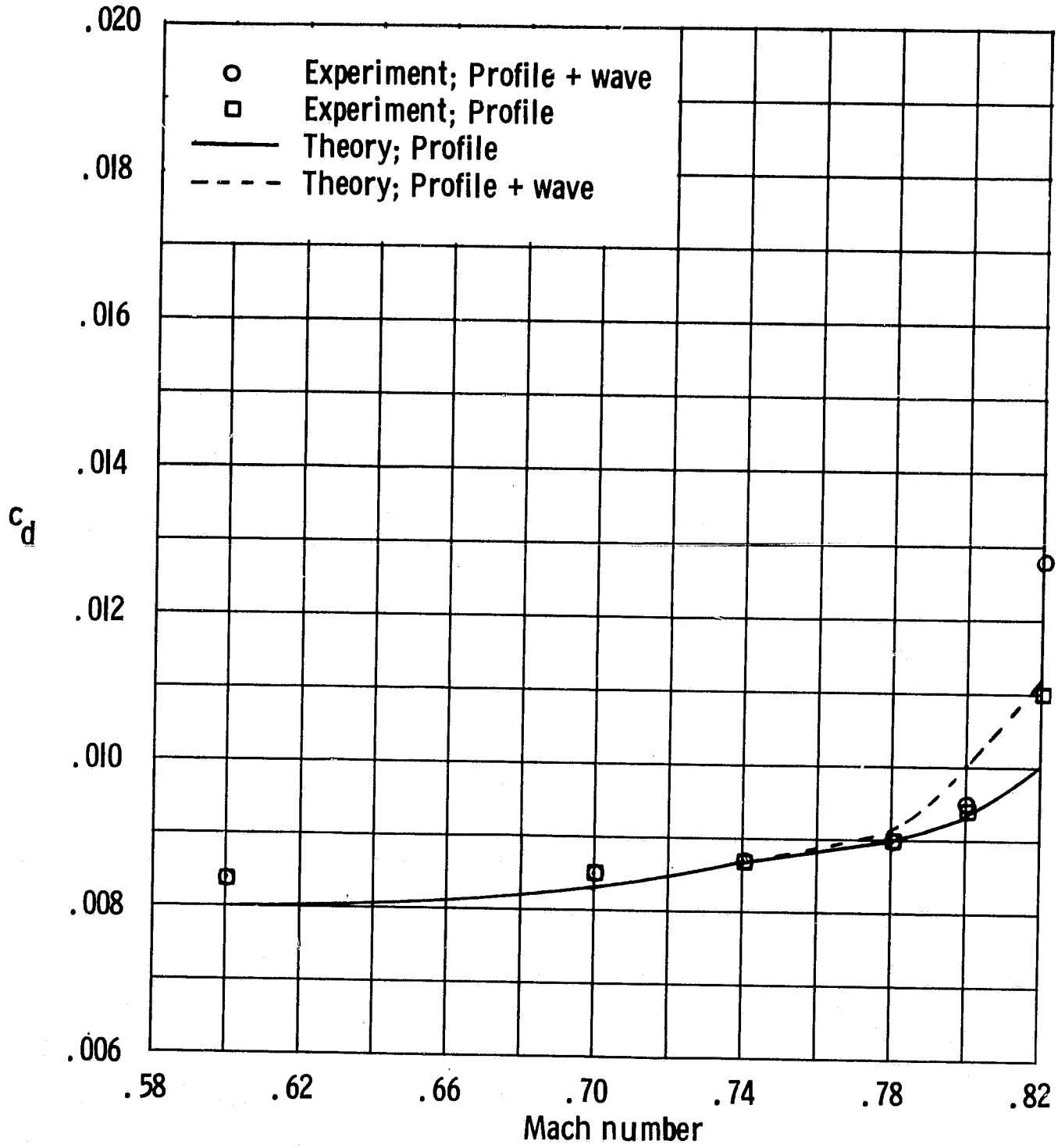

(d) $R_n = 11 \times 10^6$

Figure 5. - Concluded.

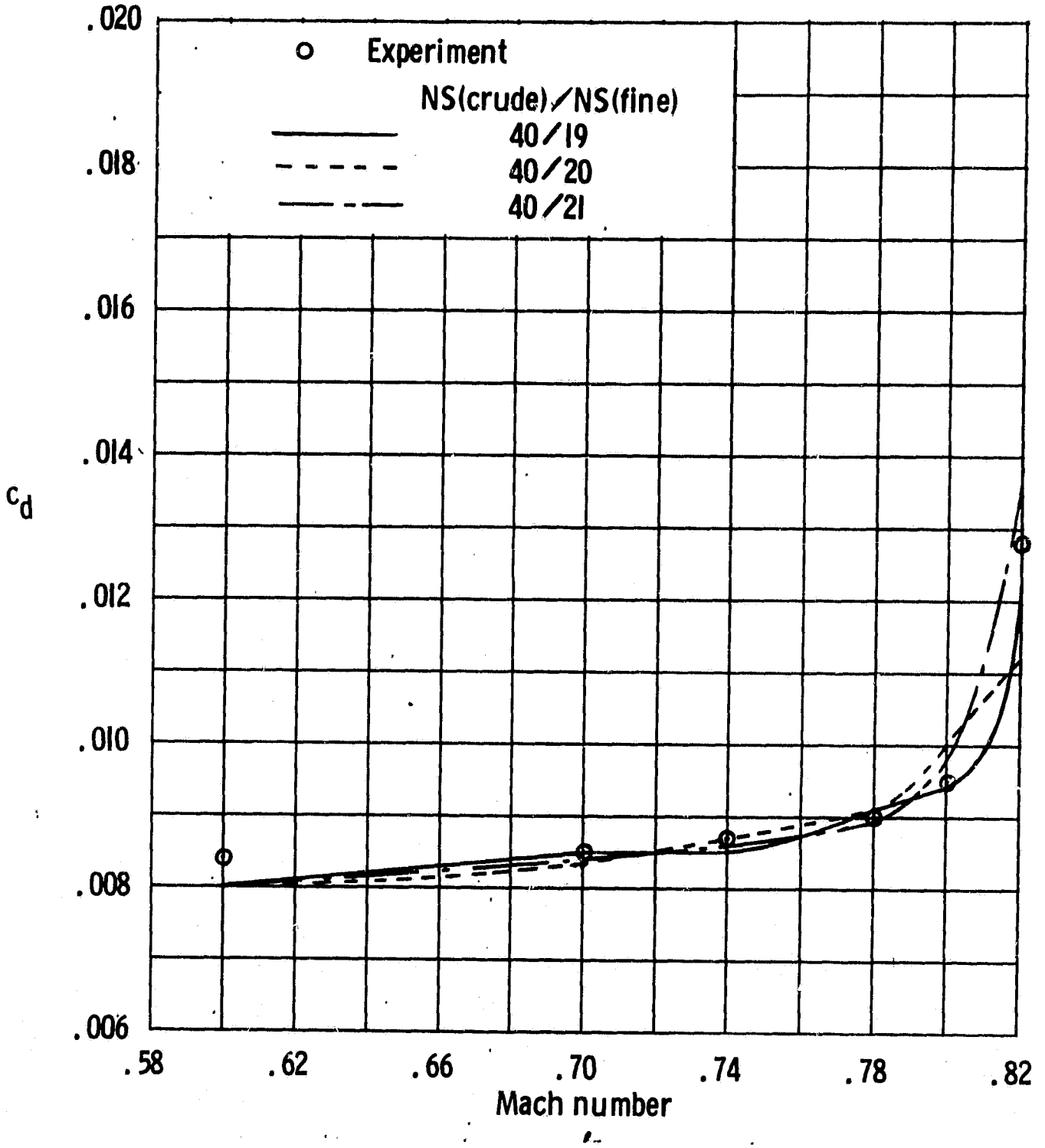

Figure 6. - Comparison of experimental and theoretical total drag characteristics. R_n = 11 x 10^6; c_n = 0.50; PCH = 0.05; MxN = 160 x 30; NS(crude) = 40; RDEL = 0.125; negative wave drag excluded.

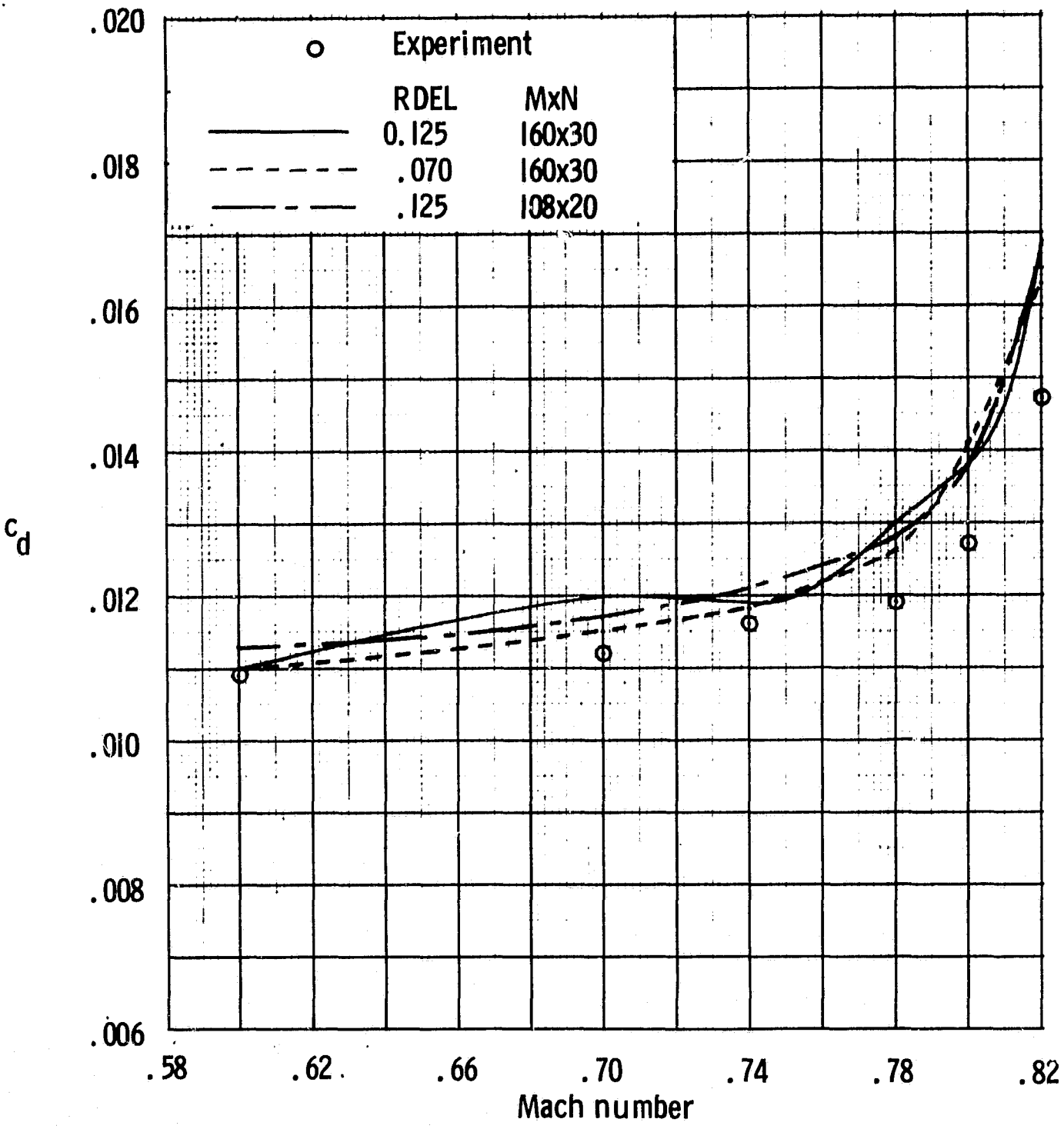

(a) $R_n = 2 \times 10^6$

Figure 7. - Comparison of experimental and theoretical total drag characteristics. c_n = 0.50; PCH = 0.05; NS(crude) = 40; NS(fine) = 20; negative wave drag excluded.

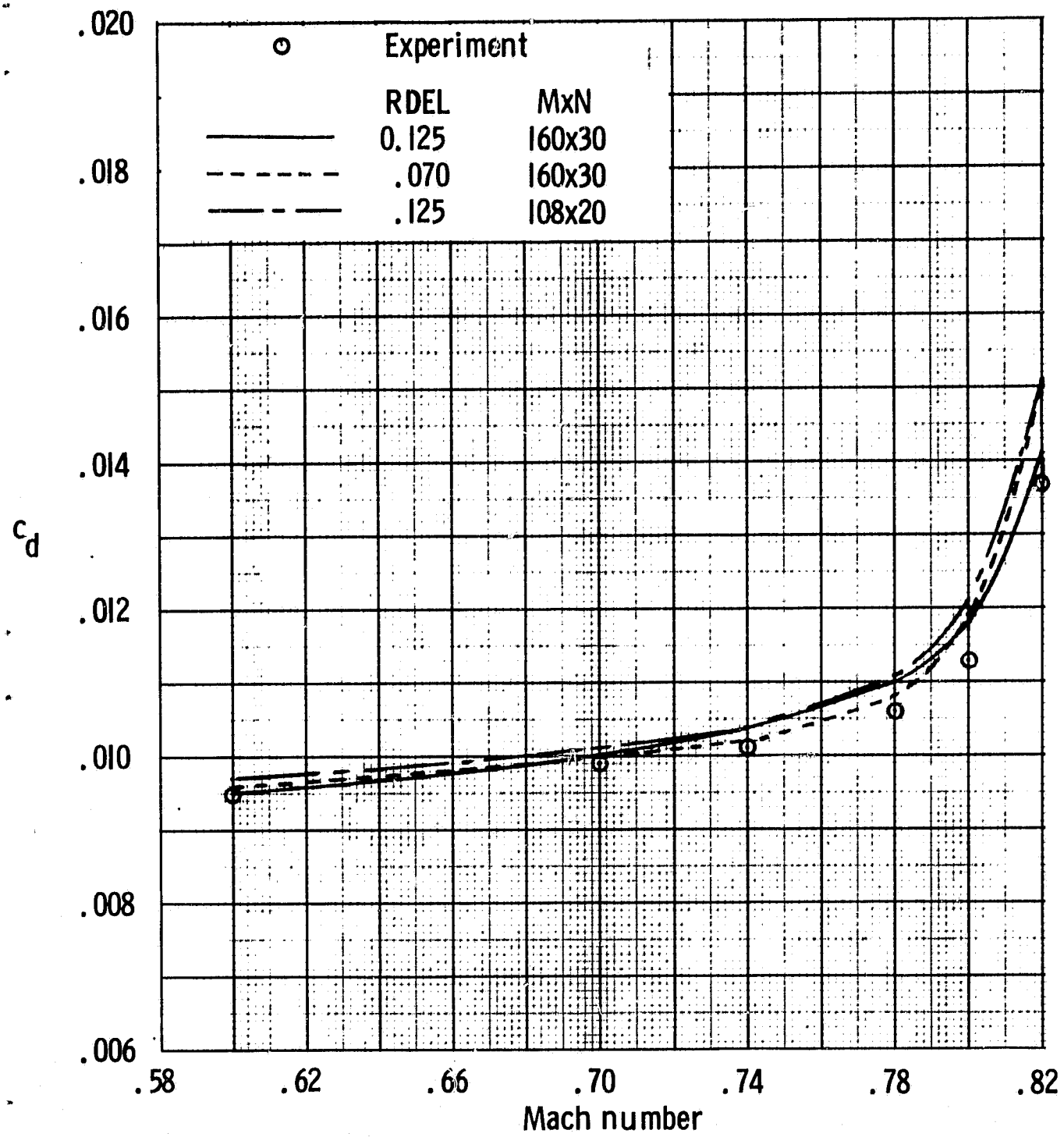

(b) $R_n = 4 \times 10^6$

Figure 7. - Continued.

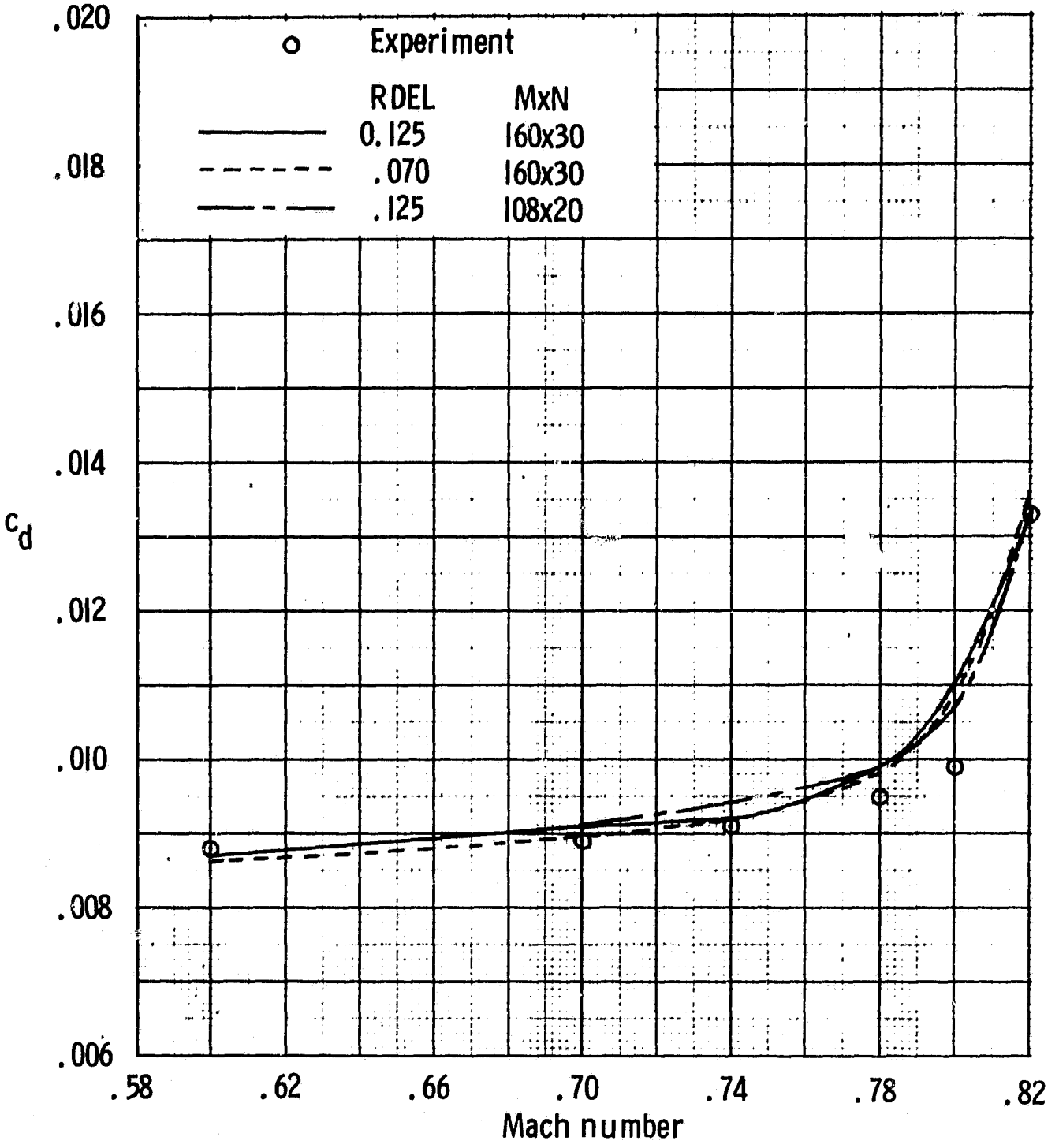

(c) $R_n = 7 \times 10^6$

Figure 7. - Continued.

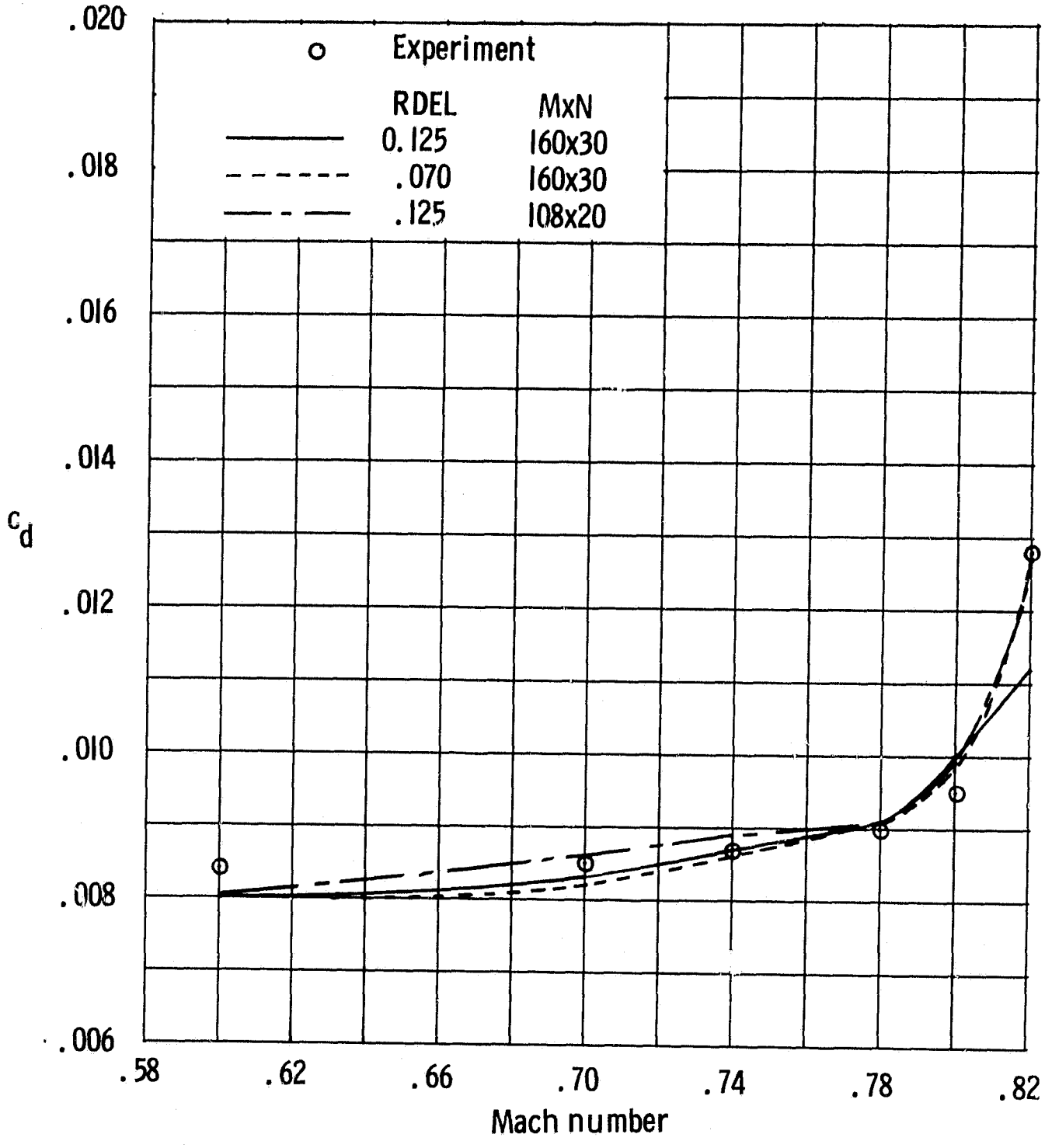

(d) $R_n = 11 \times 10^6$

Figure 7. - Concluded.

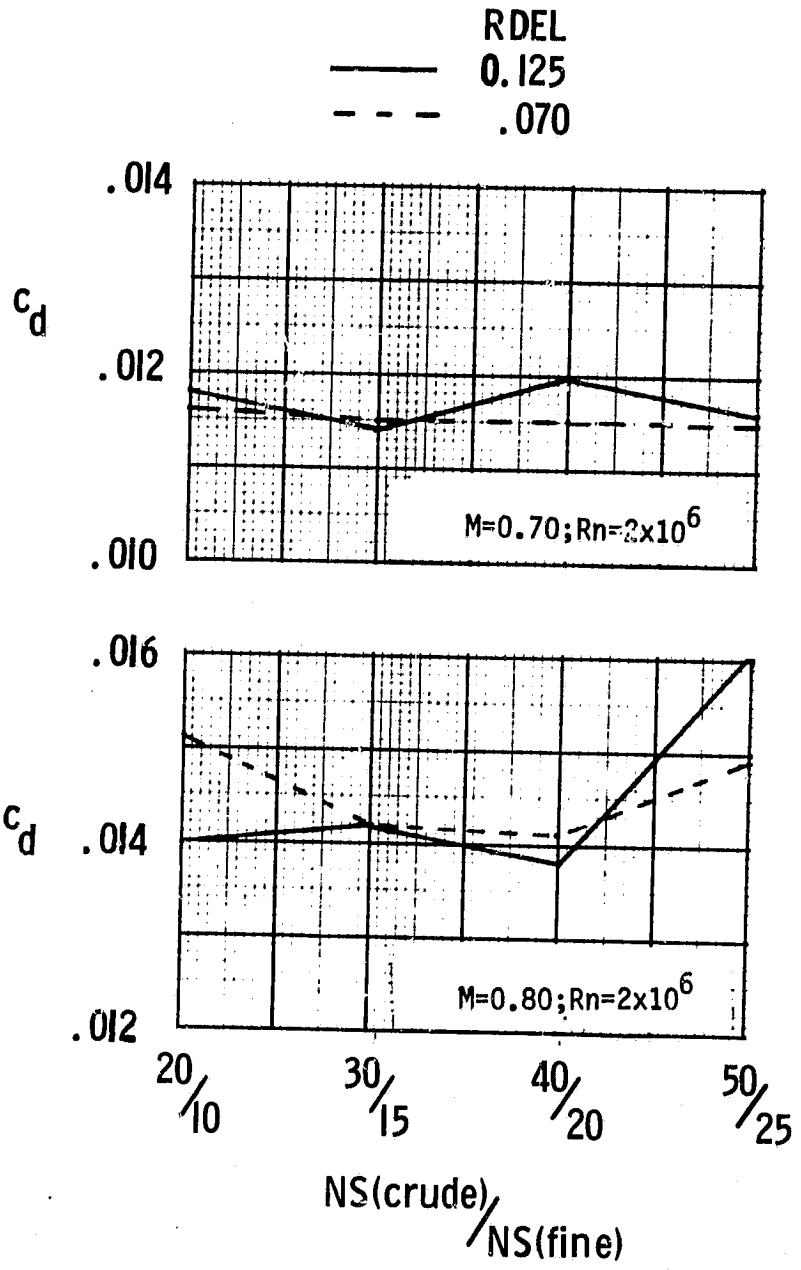

Figure 8.- Effect on theoretical total drag of number of iterative cycles at selected conditions. c_n=0.50; PCH =0.05; MxN= 160 x 30; negative wave drag excluded.

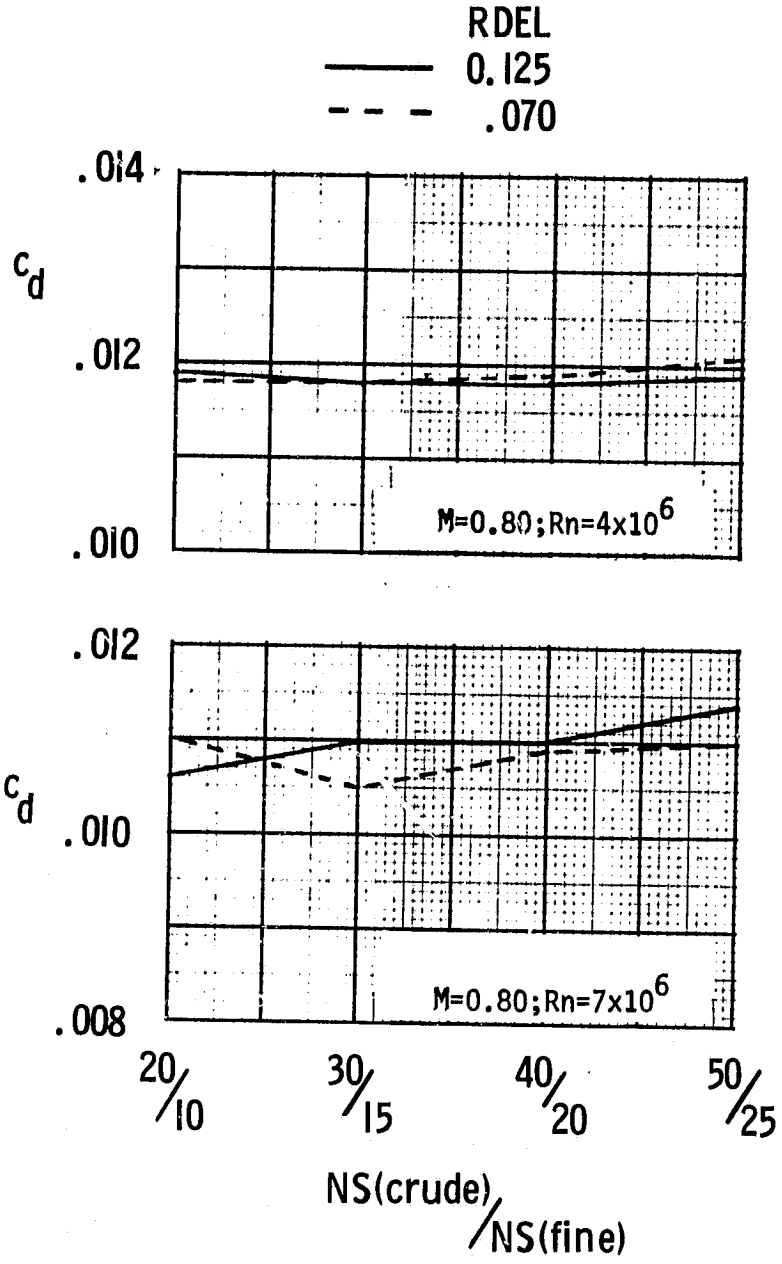

Figure 8.- Continued.

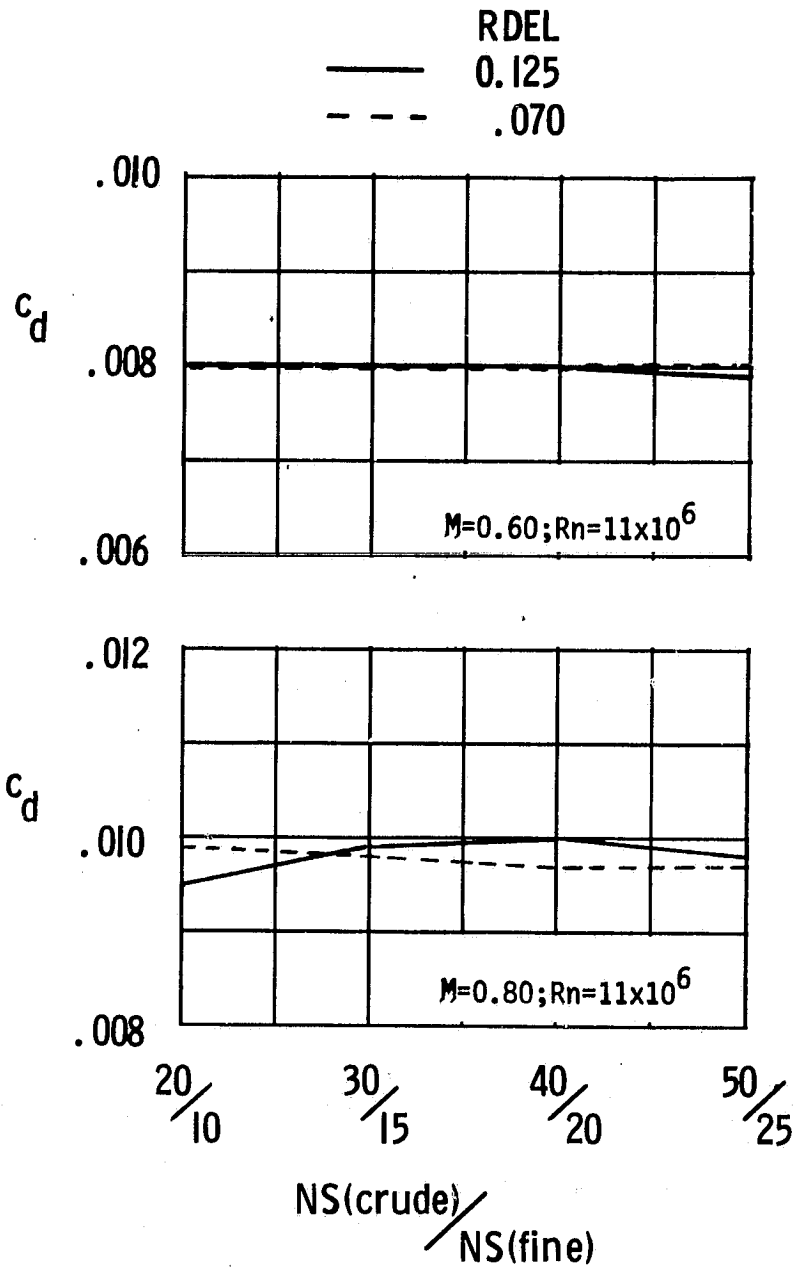

Figure 8. - Concluded.

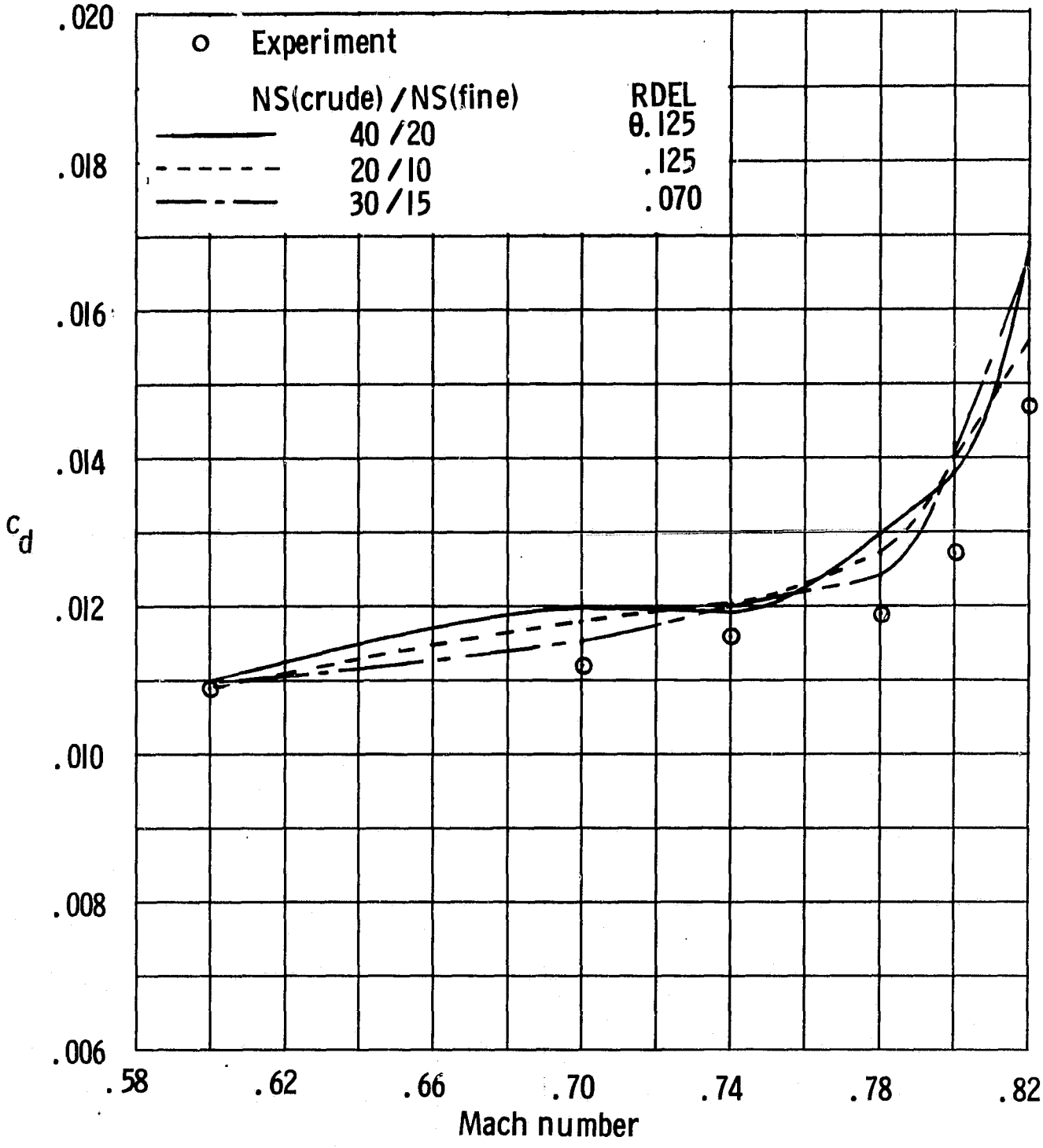

(a) $R_n = 2 \times 10^6$

Figure 9. - Comparison of experimental and theoretical total drag characteristics $c_n = 0.50$; PCH = 0.05; MxN = 160 x 30; negative wave drag excluded.

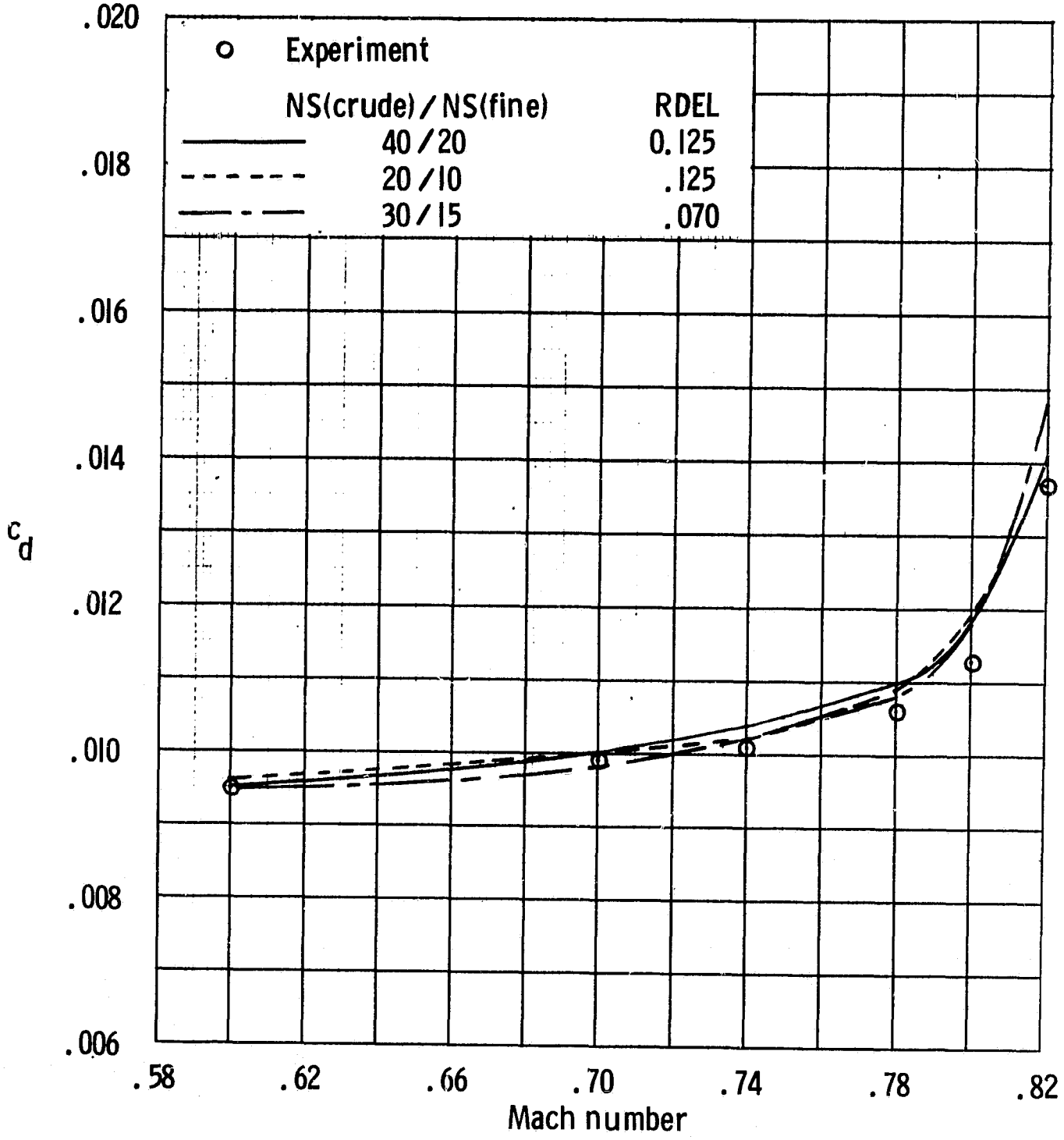

(b) $R_n = 4 \times 10^6$

Figure 9. - Continued.

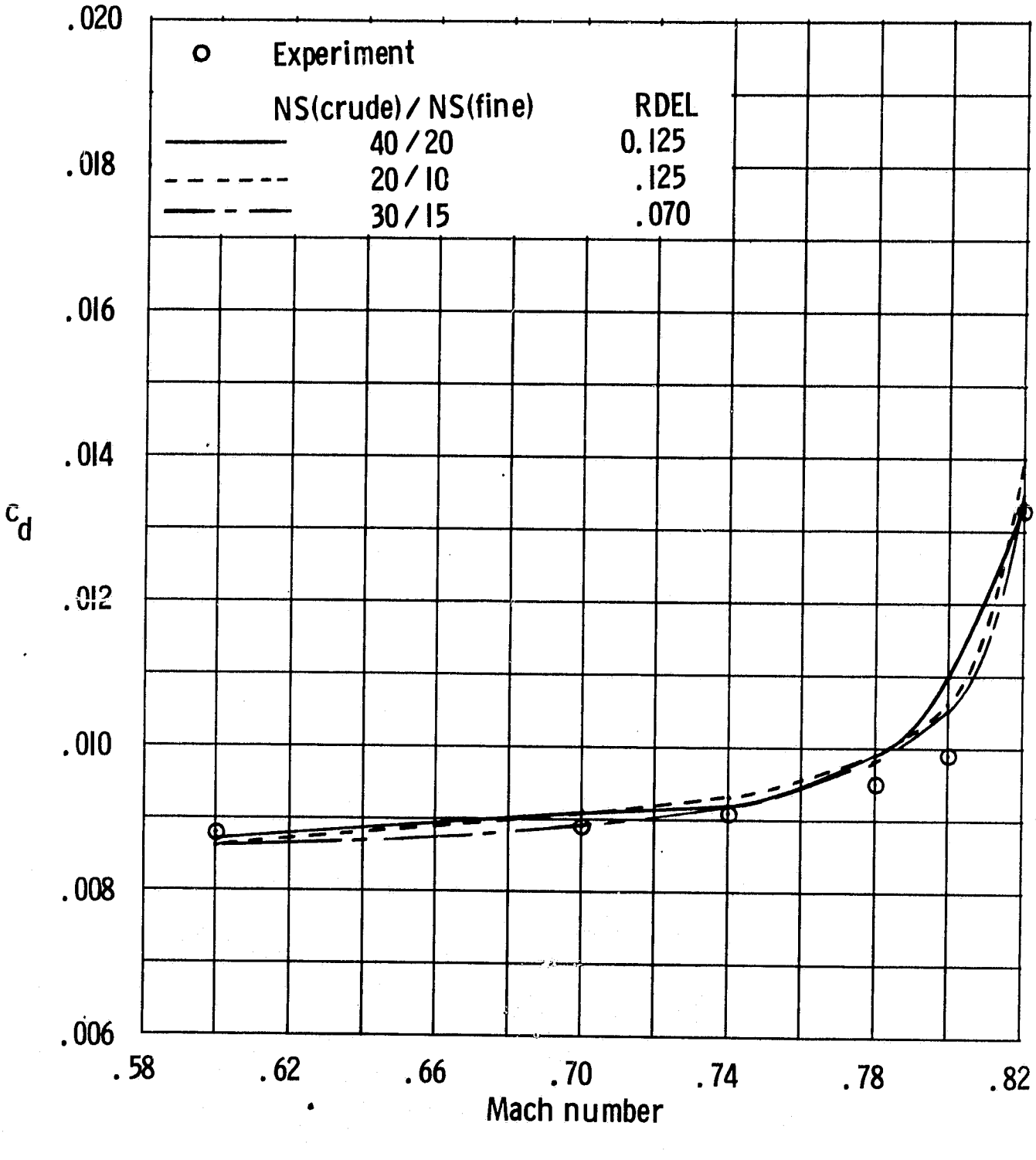

(c) $R_n = 7 \times 10^6$

Figure 9. - Continued.

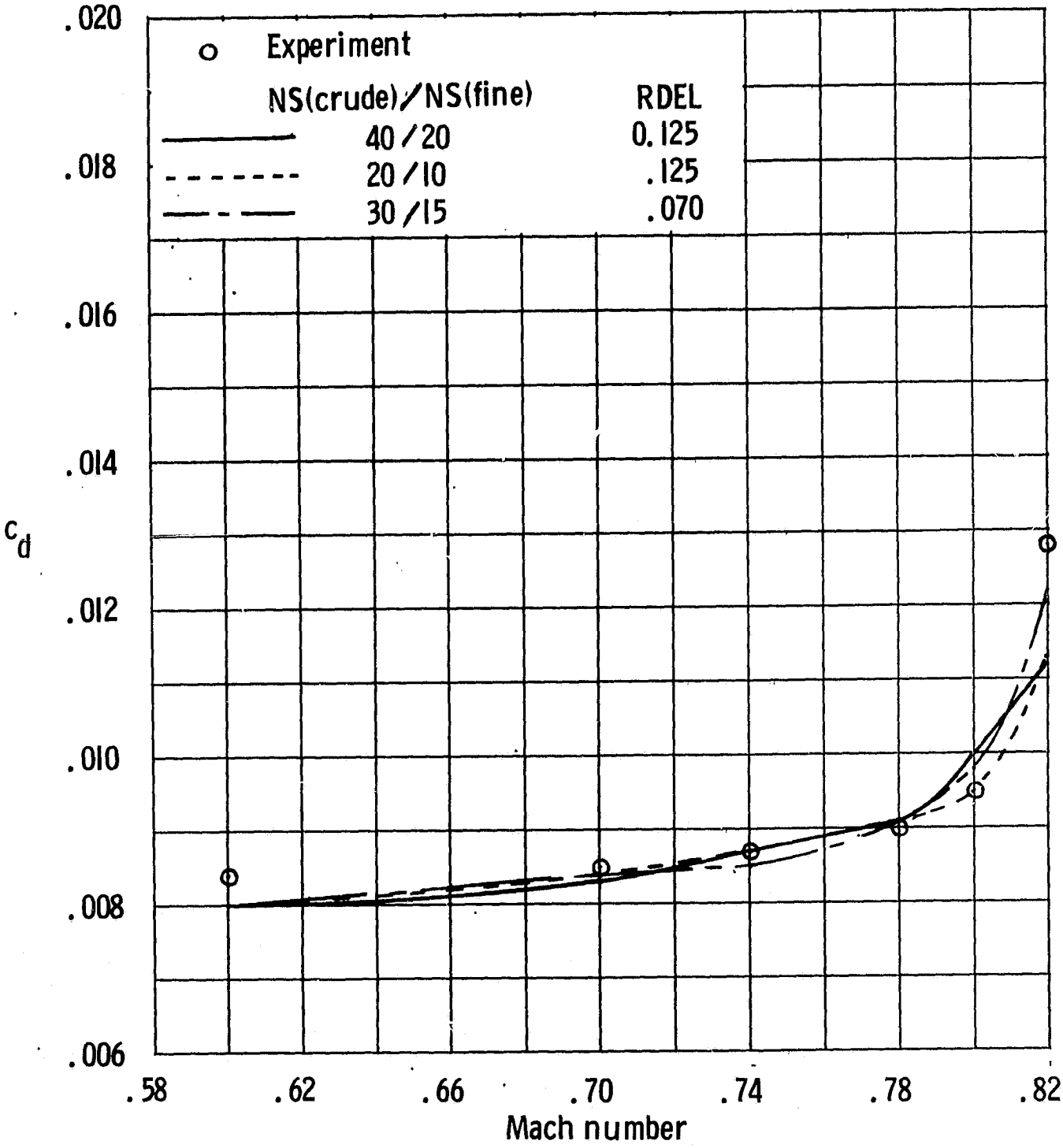

(d) $R_n = 11 \times 10^6$

Figure 9. - Concluded.